

Reply to Anonymous Referee #1

We thank the reviewer for the careful review and helpful comments. Our responses are detailed below (reviewer's comments marked in blue and our responses in black).

**Comment:** The major problem is that you should explain your results, not just describe the figures. How is the CRE effect influenced by LWP and CDNC? Why does the non-local effect exist? Especially, why the CRE maximum occurs over the Mexican gulf. These should be discussed and investigated.

**Reply:** Following the suggestion, the corresponding paragraph has been reorganized and additional description is added. We now explain how changes in cloud droplet number concentration (CDNC) and liquid water path (LWP) result in the negative SCRE in detail. The non-local effect, that is, the tendency of maximum SCRE to appear over the Gulf of Mexico is related to a more sensitive SCRE response to the larger relative change of CDNC and LWP over Gulf of Mexico compared to the land region. As shown in Fig.8 in the original manuscript, changes in both CDNC and LWP are of comparable magnitudes between Gulf of Mexico and the land region. However, given the smaller background CDNC and LWP over Gulf of Mexico, SCRE is more sensitive to changes in the two items over Gulf of Mexico than in the land region. In the revised paper, we have pointed out this phenomenon (Line 315-316) and provided an explanation (Line 337-341).

It now reads (Line 315-316):

*"It's interesting to note that the maximum SCRE tends to center around adjacent Gulf of Mexico rather than the land region."*

and (Line 320-348 ):

*"To find out the causes of the fire aerosol SCRE, fire aerosol-induced changes in cloud properties are analyzed. Given the largely insignificant change in cloud fraction (Fig. 8), the negative fire aerosol SCRE in the selected regions is mainly associated with increases in cloud droplet number concentrations (CDNC) and liquid water path (LWP). The increased CDNC due to an increase of CCN from fire aerosols (Fig. 8) leads to smaller droplet sizes, which in turn increase cloud albedo*

by enhancing backscattering (Twomey, 1977) and further affect LWP by decreasing precipitation efficiency and allowing more liquid water to accumulate (Albrecht, 1989; Ghan et al., 2012). These changes in warm cloud properties demonstrate important contributions of both aerosol first and second indirect effects to the negative SCRE. Over Southern Mexico, although changes of CDNC and LWP are of comparable magnitudes between Gulf of Mexico and the land region (Fig.8), relative changes of both items are much larger over Gulf of Mexico (Fig. S6) due to the smaller magnitudes of background CDNC and LWP here (Fig. S5), which tends to lead to a more sensitive response of SCRE. That's why the maximum SCRE over Southern Mexico is more centered around Gulf of Mexico. Changes in ice water path (IWP) and ice crystal number concentration (ICNC) can also significantly affect SCRE, but with an opposite sign and mostly in the central U.S. The decreased IWP and ICNC, which are possibly caused by fire aerosol-induced changes in the circulation (Ten Hoeve et al, 2012 and reduced coarse mode dust aerosol concentrations), are responsible for the positive SCRE in the north part of central U.S. In the south part of central U.S., the reduction of IWP and ICNC also results in a positive SCRE, which partly offsets the negative SCRE resulting from changes in warm cloud properties. This explains the weaker total negative SCRE in this region compared to the Southern Mexico region despite the more substantial increase in CDNC and LWP here. ”

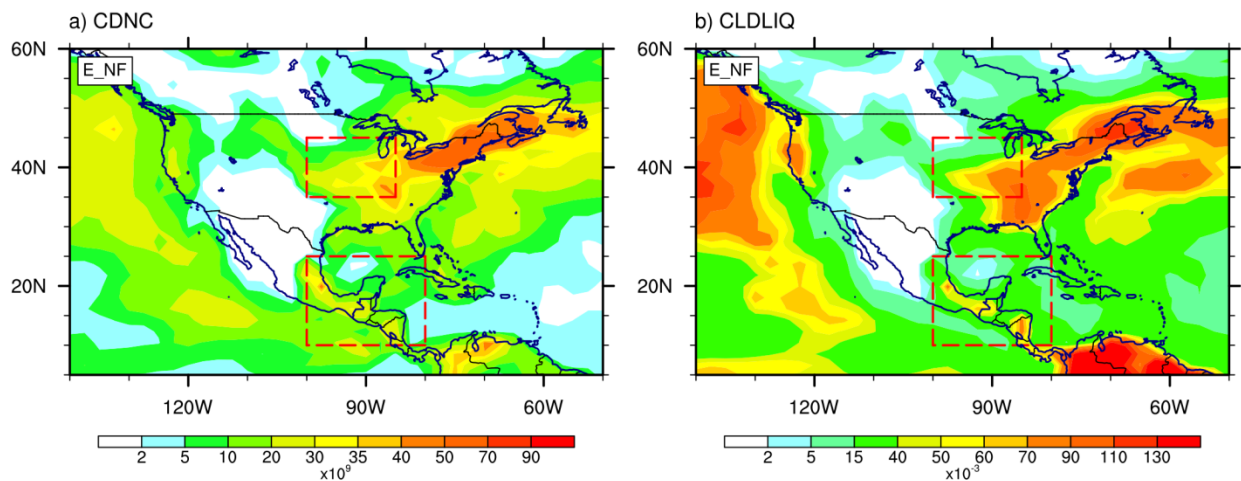


Figure S5. Spatial distributions of 10-day average (Apr. 1-10) ensemble mean a) column-integrated droplet number concentrations ( $\text{m}^{-2}$ ) and b) liquid water path ( $\text{g m}^{-2}$ ) in the E\_NF simulations.

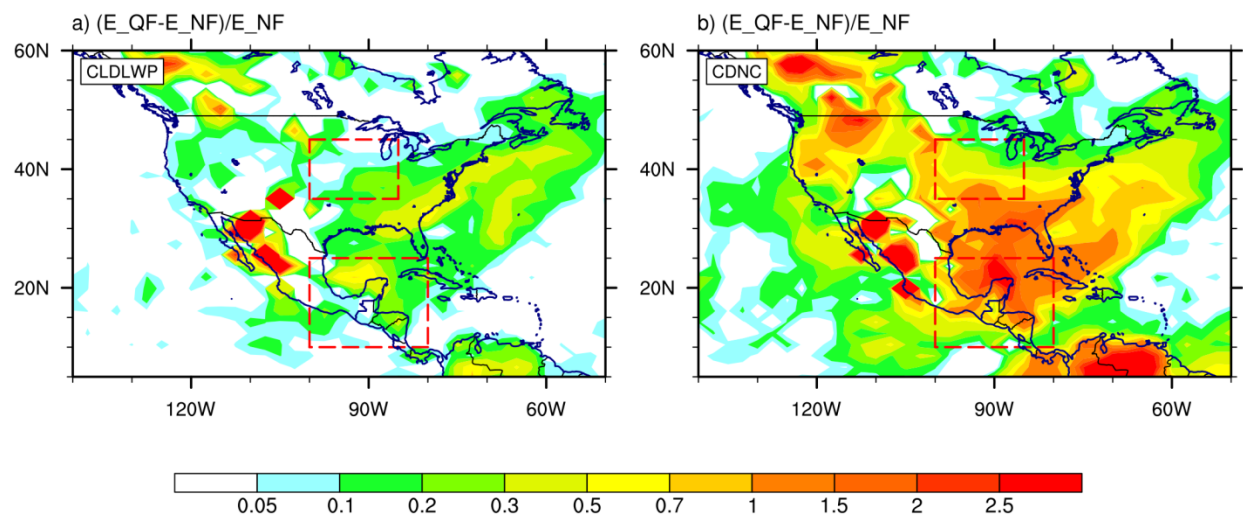


Figure S6. Relative changes of 10-day average ensemble mean cloud properties between the E\_NF and E\_QF simulations. a) cloud liquid water path, b) column-integrated droplet number concentration

**Minor comments:**

L60: studied->study

**Reply:** Done.

L370: Add "are" between "which" and "possibly";

**Reply:** Done.

L384: Same->The same;

**Reply:** Done.

L77-79: You should clarify why the indirect effect of fire aerosol deserves study.

**Reply:** Kaufman et al. (2005) and Zamora et al. (2006) show the short-term indirect effects of fire aerosols are strong based on satellite observations and aircraft measurements (Line 68-72 in the original manuscript). The fire aerosol indirect effect may significantly affect the cloud formation and radiative balance near wildfire burning region. We now explicitly mention the

significant radiative effect of fire aerosol indirect effect in the previous paragraph (Line 65-66) to emphasize this as one motivation of our study. We further pointed out in this paragraph the current lack of model simulations of short-term fire aerosol indirect effects, which is another motivation of our work.

[L101-103: What's the difference between nudging horizontal wind and temperature.](#)

**Reply:** Nudging the horizontal winds will constrain the circulation towards reanalysis, but the thermodynamical features are not directly affected. If temperature is nudged strongly (i.e. use small relaxation time scale) too, the heating/cooling introduced by nudging may affect large scale vertical motion and the parameterized convection. In our study, horizontal wind nudging was applied to constrain the large scale circulations, thus a shorter relaxation time scale of 6 hour is adopted. On the other hand, we only used very weak temperature nudging (much longer relaxation time scale) and perturbed the nudging time scale gently to create ensembles. A much longer relaxation time scale of about 10 days is used. We have clarified this difference in the revised paper. Time scales of wind nudging and temperature nudging are now explicitly provided in the corresponding paragraph. The text reads (Line 92): *“Horizontal winds were nudged towards 6-hourly reanalysis to constrain the large-scale circulation”* and (Line 96): *“we also employed very weak temperature nudging (~10days) in combination with ensembles to quantify the uncertainty. More details of the nudging setup are described in section 2.3.”*

[L297-503: How you can get the conclusion that at least 9 members are needed from Fig. 14. You need to quantify the results.](#)

**Reply:** Thanks for the suggestions. The number 9 in the discussion paper was determined by simple visual comparison. As shown in Fig.14b, discrepancies in the ensemble mean fire aerosol SCRE are substantial when the number of ensemble members (N) is smaller than 8. We agree it is better to determine the minimum required ensemble number in a quantitative way. We now use results from the 20-member ensemble simulations as a reference to evaluate the results from ensemble simulations with varying N. For a specific N, the root mean square error (RMSE) of the ensemble mean SCRE during April 1-10 is chosen to quantify the deviation of the simulated ensemble mean from the reference value. It is calculated as the standard deviation of the differences between the daily ensemble mean SCRE in the N-member simulation and the 20-

member simulation. To get robust results, for each N, we randomly sample N members from the 20 members for 1000 times and evaluated the performance of the 1000 groups (each group has N members) to avoid the influence of limited sampling. Figure 15 shows that both the RMSE of ensemble mean SCRE and the difference of RMSE between the 1000 groups of simulations (for each N) decrease with increasing N. The minimum number of N required is determined when the 90<sup>th</sup> percentile of RMSE is smaller than a threshold RMSE. Without a good reference, we set the threshold RMSE to 20% ( $0.566 \text{ W m}^{-2}$ ) of the reference 10-day mean SCRE ( $-2.83 \text{ W m}^{-2}$ ). As shown in Fig.15, at least 11 members are needed to meet this criterion. We've refined the conclusion regarding the total number of ensembles needed in the revised paper. The corresponding paragraph now reads (Line 395-408):

*“However, discrepancies in the ensemble mean fire aerosol SCRE (Fig. 14b) are substantial when the number of ensemble members is small. The same is true for the ensemble spread of fire aerosol SCRE (Fig.S8). In order to quantify the discrepancies of the simulated SCRE, we chose the ensemble mean SCRE in the 20-member simulation as a reference and use the root mean square errors (RMSE) of the ensemble mean SCRE in the N-member simulation to quantify the deviation of the simulated SCRE from the reference value. It is calculated as the standard deviation of the differences between the daily ensemble mean SCRE in the N-member simulation and the 20-member simulation. For each N, we randomly sampled 1000 times from the 20 members to help reduce the influence from limited sampling. Figure 15 shows that both the RMSE of ensemble mean SCRE and the difference of RMSE between the 1000 groups of simulations (for each N) decrease with increasing N. The minimum number of N required is determined when the 90<sup>th</sup> percentile of RMSE is smaller than a threshold RMSE. Without a good reference, we set the threshold RMSE to 20% ( $0.566 \text{ W m}^{-2}$ ) of the reference 10-day mean SCRE ( $-2.83 \text{ W m}^{-2}$ ). As shown in Fig.15, at least 11 members are needed to meet this criterion.”*

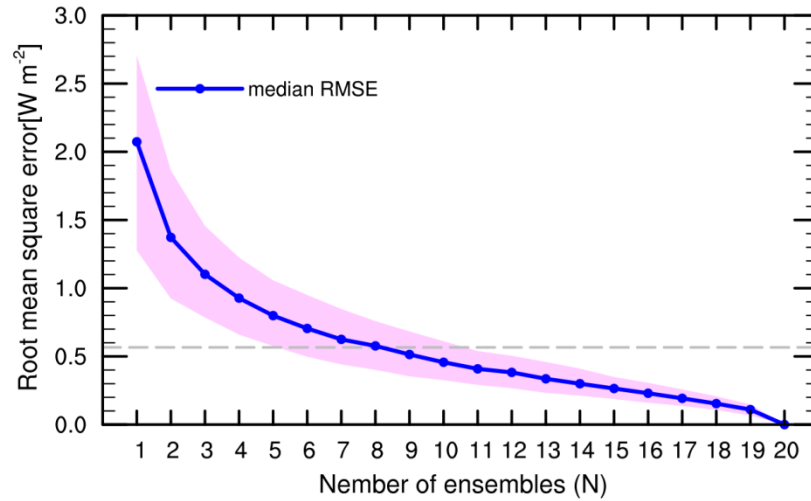


Figure 15 Root mean square errors (RMSE) of the ensemble mean of the regional mean fire aerosol SCRE during April 1-10 over Southern Mexico in simulations with different total number of ensemble members (N). The blue line represents the median RMSE of the 1000 groups (each group has N members/simulations). The grey line represents the threshold RMSE. Shaded area denotes the range between the 10<sup>th</sup> and 90<sup>th</sup> percentiles.

Reply to Anonymous Referee #2

We thank the reviewer for the helpful and constructive comments. Our point-by-point responses are provided below (reviewer's comments marked in blue and our responses in black).

This paper studies the direct/indirect aerosol effect from fires using CAM5 with nudged horizontal wind speed and/or nudged temperature. Overall the approach is sound and the paper is well written. Yet it still needs some major clarifications before it is accepted for publication.

**General comments:**

Since fire emission inventories are critical to this study, please provide a table or a plot to show the BC/OC/SO<sub>2</sub> emissions from the 3 different inventories quantitatively. The colorbar in Fig. 2 is difficult to tell how bigger is the QF than the GF3/4. It seems QF emissions are at least 5 times larger than the other two. Please provide a table showing the different fire aerosol forcing components. In the introduction part, 3 different aerosol forcing are mentioned, but only direct forcing and short wave cloud forcing are presented in the result section. Please show long wave forcing and surface albedo forcing as well in the table. The initial condition for the 10-day ensemble runs is generated by S\_NF with only u and v being nudged. Temperature is not nudged for the S\_NF run. So my question is when you now include slow temperature nudging in the ensemble runs, will they go through some adjustment through the 10-day period? Or in other word, how well is the initial T compared to the T being nudged to on April 1st?

**Reply:** We have added the Table S1 to show the monthly mean and 10-day mean BC/OC/SO<sub>2</sub> emissions from the three inventories. In both regions, the factor difference between the GFED and QFED data is similar no matter whether monthly mean or 10-day mean is used for comparison. Overall, the QFEDv2.4 emissions are larger than GFED v4.1s emissions by a factor of approximately 10 in the Central U.S and a factor of approximately 3 in Southern Mexico. We mentioned in the original manuscript that “*Values of emitted BC in QFED v2.4 are larger than those in GFED v4.1s by a factor of 9.7 in the Central U.S. and a factor of 2.7 in Southern Mexico*”, but didn't specify this was based on the 10-day mean emissions. This has been clarified in the revised paper (Line 152-153).

Following the reviewer’s suggestion, we have also added Table S3 to show the different components of fire aerosol effects. As shown in Table S3, Shortwave direct radiative effect (SDRE) and shortwave cloud radiative effect (SCRE) are the major contributors to the total fire aerosol effect in both regions. The surface albedo effect is almost negligible. The E\_QF simulation shows a significant negative longwave cloud radiative effect (LCRE) in the Central U.S., which is associated with reduced ice crystal number concentrations and ice water path in the north part of this region. We have added a brief description of the negative LCRE (Line 344-345) in the revised paper. Causes of the fire aerosol effect are discussed in detail in Section 3.2.2.

The global pattern of the initial T (or the anomaly) is very similar to those in the reanalysis data but there are some regional differences. It should be noted that the horizontal wind nudging and temperature nudging are applied for different purposes. The horizontal wind nudging is used to constrain large-scale features in simulations with and w/o fire emissions to help better identify radiative forcing signal, while the weak temperature nudging conducted with gently perturbed time scale is used to generate ensemble and investigate the fire forcing uncertainty. Given its large relaxation time scale (10 to 11days compared to the 6-hourly wind nudging), the temperature nudging with small adjustments of temperature has little effect on constraining the temperature field towards reanalysis. We have added the time scale of wind and temperature nudging in Line 92 and Line 96 to clarify the difference.

Table S1 Regional mean emissions of fire aerosols in April, 2009 from three emission inventories (Unit:  $\times 10^{-12}$  kg  $m^{-2}s^{-1}$ ). Numbers in the parentheses show results averaged in April 1-10.

	BC		OC		SO <sub>2</sub>	
	Central U.S.	Southern Mexico	Central U.S.	Southern Mexico	Central U.S.	Southern Mexico
GFED v3.1	0.25(0.38)	0.69(0.82)	1.82(3.58)	5.60(6.77)	1.35(2.01)	3.69(4.35)
GFED v4.1s	0.23(0.34)	1.17(1.44)	1.75(3.24)	8.80(10.76)	1.21(1.81)	6.25(7.69)
QFED v2.4	2.63(3.29)	3.87(3.87)	23.54(32.25)	36.81(36.58)	14.04(17.59)	20.62(20.65)



Table S3 Regional mean total AOD, fire AOD (differences in AOD between simulations with and without fire) and radiative effects of fire aerosols during April 1-10, 2009 in group B simulations (Unit:  $W m^{-2}$ ). Total fire aerosol radiative effect is decomposed into shortwave direct radiative effect (SDRE), shortwave cloud radiative effect (SCRE), longwave cloud radiative effect (LCRE) and surface albedo effect (SAE).

	Total AOD	Fire AOD	SDRE	SCRE	LCRE	Total SAE
Central U.S.						
E_NF	0.047					
E_GF3	0.050	0.003	0.02	-0.86	0.04	0.02
E_GF4	0.050	0.003	-0.01	-0.39	0.002	-0.003
E_QF	0.08	0.033	-0.10	-0.56	-0.76	0.12
Southern Mexico						
E_NF	0.135					
E_GF3	0.149	0.014	-0.18	-1.91	-0.21	0.06
E_GF4	0.153	0.018	-0.20	-2.06	-0.23	0.11
E_QF	0.202	0.067	-0.86	-3.02	-0.47	0.14

### Specific comments:

**Comment:** Abstract: why no forcing numbers are provided here. It is expected to see direct forcing and net indirect forcing rather than some changes in the short wave cloud forcing.

**Reply:** We have added forcing numbers in the revised paper and the text reads (Line 30-32) :  
*“Strong negative shortwave cloud radiative effect (SCRE) covers almost the entire Southern Mexico with a 10-day regional mean value of  $-3.02W m^{-2}$ . Over the Central U.S, comparable positive and negative SCRE of approximately  $2W m^{-2}$  appear in the north and south part of the region respectively. “*

**Comment:** Line 62-76: Please show what these forcings are. Direct or indirect?

**Reply:** We have specified direct or indirect effect (Lines 60-67).

**Comment:** Line 103: Please provide relaxation time for the very weak temperature nudging

**Reply:** The nudging time scale has been added and it now reads (Line 96): *“Even for short simulations, small perturbations of meteorological states might have large impact on the local aerosol and cloud properties, thus bring uncertainty to the aerosol forcing estimate. Therefore, in our simulations, we also employed very weak temperature nudging (~10days) in combination with ensembles to quantify the uncertainty. More details of the nudging setup are described in Section 2.3.”*

**Comment:** Line 131-132: Please show or elaborate how you convert monthly mean emissions to daily emissions?

**Reply:** The GFED website (<http://www.globalfiredata.org/data.html>) provides monthly emission data and daily scalars to convert the monthly emission to daily emission. We have added following descriptions in Section 2.2 (Line 121-123): *“The daily emission data is obtained using daily scalars (<http://www.globalfiredata.org/data.html>) to distribute monthly emissions over the days and is only available from 2003 onwards.”*

**Comment:** Line 138-142: Does the CAM5 default/background emission already include fire emission? Or did you remove fire emissions from the CAM5’s emission files if there is any?

**Reply:** We didn’t use the default climatological monthly mean fire emission in the CAM5 model. We replaced the original fire emission with the daily emission dataset mentioned in this study.

**Comment:** Line220-226: Please define these forcings with a few sentences rather than refer readers to Ghan 2013.

**Reply:** We have added a few sentences to elaborate the calculation of fire aerosol effect. Fire aerosol DRE, CRE and surface albedo effect are first defined as changes in total aerosol forcing, cloud forcing and surface albedo forcing between simulations with and without fire emissions. Then, a detailed description of the calculation of total aerosol forcing, cloud forcing and surface albedo forcing in the fire (or no fire) simulation is provided. The text now reads (Line 194-204)

*“Similar to Jiang et al. (2016), our calculations are based on the work of Ghan et al. (2012) and Ghan (2013). Fire aerosol DRE, CRE and surface albedo effect are defined as fire induced changes in aerosol forcing, cloud forcing, and surface albedo forcing respectively, and are calculated as the difference of each item between simulations with and without fire emissions (denoted by  $\Delta$ ). In each simulation, aerosol forcing was defined as the difference between all-sky and clean-sky TOA radiative fluxes ( $F - F_{clean}$ ). Cloud forcing was defined as the difference between all-sky and clear sky TOA radiative fluxes under clean-sky conditions ( $F_{clean} - F_{clean,clear}$ ). The rest were related to surface albedo forcing ( $F_{clean,clear}$ ). Thus fire aerosol DRE, CRE, and surface albedo effect were expressed as  $\Delta(F - F_{clean})$ ,  $\Delta(F_{clean} - F_{clean,clear})$ , and  $\Delta F_{clean,clear}$ , respectively. More details about the method can be found in section 2 of Ghan (2013). CRE includes contributions of both aerosol indirect effect and aerosol semi-direct effect but was analyzed as a single term (i.e., the sum).”*

**Comment:** Line 238: Please explain what "LEV 2.0 cloud-screened" is.

**Reply:** The AERONET web page (<https://aeronet.gsfc.nasa.gov/>) provides both original raw data and processed data at AERONET sites. The LEV 2.0 AOD is the processed data based on a cloud-screening algorithm (Smirnov et al. 2000). This information is now added (Line 214-215): *“LEV 2.0 cloud-screened all points AOD at 500 nm and 675 nm was used to generate hourly AOD at 550 nm, which are the processed data based on a cloud-screening algorithm (Smirnov et al. 2000)”*

**Comment:** How much does the fire emitted aerosols contribute to the total AOD? It would be helpful to show some estimate of the contributions from fire emitted aerosols and other background aerosols. I realized you presented background AOD and fire AOD later in Fig. 6. But it would be more helpful if you can present some data here when you quote the need to increase the fire emissions by a factor of 1-3. And please explain why increasing the fire emission by a factor 1-3 could then make the simulated AOD large enough to compare with the reanalysis. It seems it is still unlikely to me.

We have added Table S2 showing total AOD, fire AOD and the contributions of fire AOD for reference in the revised paper. The following description is added (Line 245-246): *“Fire aerosols-*

*induced AOD increase accounts for 8.1% (S\_GF3), 11.2% (S\_GF4) and 48.8% (S\_QF) of the background AOD (Table S2)."*

In the original manuscript, we quoted the need to increase the emissions by a factor of 1-3 mainly in order to show that the underestimation of AOD in simulations driven by GFED data is common. Thus the results in this study are consistent with previous studies. We didn't mean to imply that the scale factor from 1-3 can also be applied in this case. In fact, the scale factors are regionally-specific. In the work of Tosca et al. (2013), they derived the scale factors by computing the ordinary least squares regression between the simulated AOD and the observed AOD (MISR and MODIS) for those months over 1997-2009 that cumulatively contributed to 80% of regional fire emissions. In the selected four regions in their work including South America, South Africa, equatorial Asia and boreal North America, the scale factors range from 1-3. For the selected region and period in this study, larger scale factors are needed to make simulated AOD in agreement with the NRL and MACC reanalysis data. However, it's worth noting that both reanalysis data shows a positive bias when compared to AERONET data especially in the Central U.S, while a good agreement is found between the simulated AOD in S\_QF and AERONET observations (shown in Fig.4 in the original manuscript). Therefore a scale factor that brings the simulated AOD in the GFED forced simulations comparable to that in the QFED forced simulation might be more reasonable. We have performed sensitivity analysis by performing simulations driven by varying magnitudes of fire emissions (0, 1, 2, 5 times the emission). Results show that changes of fire AOD is proportional to changes in fire emissions. Therefore, the conclusion of a scale factor from 1-3 to match observations still holds in Southern Mexico, but a much larger scale factor of about 10 is needed in the Central U.S. We reorganized corresponding sentences in the revised paper to avoid ambiguity (Line 239-241): "*Previous studies have found the underestimation of AOD in simulations with GFED emissions and suggested the need to scale up GFED emissions by a factor of 1-3 to match the observed AOD (Tosca et al., 2013). This is consistent with the large negative bias in the simulation S\_GF3 and S\_GF4.*" and clarified that (Line 242): "*However, a much larger scale factor might be needed in this case.*"

Table S2 Regional mean total AOD, fire AOD (difference in total AOD between simulations with and without fire) and the contributions of fire AOD (fire AOD divided by total AOD in the S\_NF simulation)during April, 2009 in group A simulations.

	Central U.S.			Southern Mexico		
	Total AOD	Fire AOD	Percentage	Total AOD	Fire AOD	Percentage
S_NF	0.066			0.130		
S_GF3	0.068	0.002	3.42%	0.141	0.011	8.10%
S_GF4	0.070	0.004	5.63%	0.145	0.015	11.20%
S_QF	0.099	0.033	49.33%	0.194	0.064	48.84%

**Comment:** Line 357-358: It is confusing here. Please consider revising.

**Reply:** The text is revised as follows (Line 317-319): *“In the central U.S, despite moderate fire aerosol SDRE, a positive fire aerosol SCRE exceeding  $2 W m^{-2}$  appears in the north part of the region while a comparable negative SCRE appears in the south part of the region.”* Discussions on these results are provided in the next paragraph.

**Comment:** In the simulations with nudged U and V, the circulation is constrained. So it seems the circulation change may be small enough. Then use this to explain to change of ice clouds. I suspect the coarse mode dust number may be smaller and this may contribute to the decrease of produced ice number since the ice nuclei number (dust) is smaller. Need further investigation here.

**Reply:** We thank the reviewer for the helpful comment. Yes. The coarse mode dust concentration is reduced in the S\_QF simulation (Figure S7), thus it is one of the possible causes for the reduced cloud ice amount and cloud ice number concentration. However, note that the location of maximum cloud ice decrease is a bit different from the location of maximum coarse mode dust concentration. In addition, a rough estimate of the change in coarse mode dust number concentration is on the order of  $10^{-3} kg^{-1}$  when using dust aerosol density of about  $2.5 g cm^{-3}$  and a coarse mode diameter of about  $2\mu m$ . This means, even assuming that all the

reduced coarse mode dust aerosols are effective ice nuclei, the resulting decrease in cloud ice number concentration from heterogeneous nucleation is still one order smaller than that shown in Figure S7 b).

Although horizontal wind is nudged in this study, changes in the vertical heating profile (e.g. due to BC absorption) would affect the distribution of large-scale vertical velocity. We notice a substantial change in the vertical velocity right below the location with maximum reduced ice cloud. Positive values in Figure S7e) represent downward motions induced by fire aerosols, which lead to a reduced vertical transport of moisture to the upper levels and will suppress the homogeneous ice nucleation there.

We have clarified this in the revised paper and the text now reads (Line 342-344): “*The decreased IWP and ICNC, which are possibly caused by fire aerosol-induced changes in the circulation (Ten Hoeve et al, 2012) and reduced coarse mode dust aerosol concentrations (Fig.S7), are responsible for the positive SCRE in the north part of central U.S*”

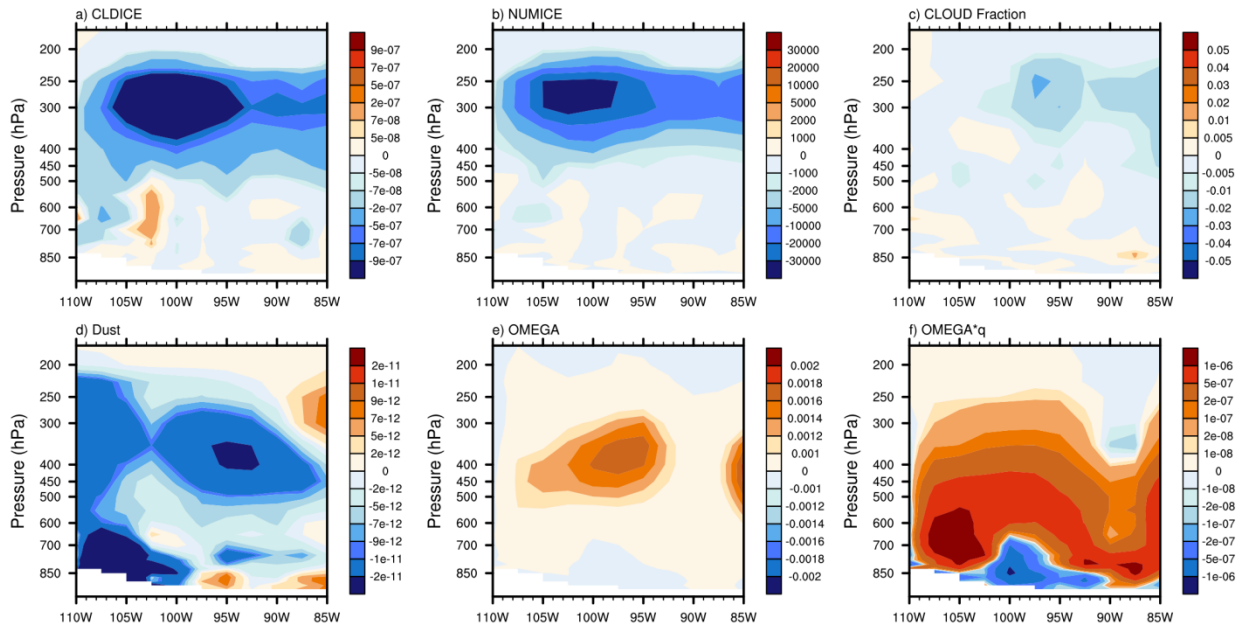


Figure S7. Pressure and longitude distribution of meridional mean ( $40-45^{\circ} \text{N}$ ) difference of 10-day average (April 1 -10) ensemble mean between simulation E\_NF and E\_QF: a) cloud ice amount ( $\text{kg} \cdot \text{kg}^{-1}$ ) b) cloud ice number concentration ( $\text{kg}^{-1}$ ) c) cloud fraction (1) d) Coarse mode dust concentration ( $\text{kg} \cdot \text{kg}^{-1}$ ) e) vertical velocity ( $\text{Pa} \cdot \text{s}^{-1}$ ) f) vertical moisture transport ( $\text{kg} \cdot \text{kg}^{-1} \cdot \text{Pa} \cdot \text{s}^{-1}$ )

**Comment:** Line 385: make it clear it is SW cloud forcing

Reply: Corresponding sentences have been revised (Line 357-359).

**Comment:** Line 420: Why quote Fig. 3 here? I think Fig.3 shows results from Group A not from ensemble runs.

Reply: Fig.3 shows the results from both group A (for the whole month) and group B (for the first 10 days) simulations. Results from the ensemble runs are indicated by the range between the maximum and minimum values among ensemble members with darker colors. However, since the simulated AOD is barely distinguishable among members, and between two groups of simulations, the line and the shaded areas almost overlap. The shaded range can be more easily seen in Fig.3 b) by comparing the difference between first 10 days and the rest 20 days. We mentioned in the original manuscript that the shaded areas are very narrow. We have added following sentences in the caption of Fig.3 to further clarify this *“For the single-member simulation and the ensemble simulation driven by same fire emission, the shaded area and the solid line almost overlap given the barely indistinguishable AOD between ensemble members and the corresponding Group A simulation.”*

**Comment:** Line 430-432: How is the spread calculated for different N? Also how do you select the ensemble member for each different N? I suspect the number 9 required to converge may be different if the ensemble members for different N are constructed differently

Reply:

- 1) The spread is calculated as the sample standard deviation of ensemble members. For a specific N (number of ensemble members), values of ensemble members are denoted as  $X_i$  ( $i = 1, 2, \dots, N$ ). Ensemble mean is calculated as  $\bar{X} = \frac{1}{N} \sum_{i=1}^N X_i$ . Ensemble spread is calculated as  $\sigma = \sqrt{\frac{1}{N-1} \sum_{i=1}^N (X_i - \bar{X})^2}$ .
- 2) We performed a group of simulations with a total of 20 members. They are generated by implementing a weak temperature nudging with relaxation time scale ranging from (10 ~11.9 days with an interval of 0.1 day). For a specific N, the first N members are chosen

in calculation, that is, members with relaxation time scale ranging from  $(10 \sim 10 + 0.1(N-1))$  days).

- 3) We thank the reviewer for this insightful comment, which has allowed us to further validate the robustness of our results. A quantitative way is now provided to determine the minimum numbers of ensemble members required in this case study. We now use results from the 20-member ensemble simulations as a reference to evaluate the results from ensemble simulations with varying N. For a specific N, the root mean square error (RMSE) of the ensemble mean SCRE during April 1-10 is used to quantify the deviation of the simulated ensemble mean from the reference value. It is calculated as the standard deviation of the differences between the daily ensemble mean SCRE in the N-member simulation and the 20-member simulation. To get robust results, for each N, we randomly sample N members from the 20 members for 1000 times and evaluated the performance of the 1000 groups (each group has N members) to avoid the influence of limited sampling. Figure 15 shows that both the RMSE of ensemble mean SCRE and the difference of RMSE between the 1000 groups of simulations (for each N) decrease with increasing N. The minimum number of N required is determined when the 90<sup>th</sup> percentile of RMSE is smaller than a threshold RMSE. Without a good reference, we set the threshold RMSE to 20% ( $0.566W m^{-2}$ ) of the reference 10-day mean SCRE ( $-2.83 W m^{-2}$ ). As shown in Fig.15, at least 11 members are needed to meet this criterion. We've refined the conclusion regarding the total number of ensembles needed in the revised paper. Corresponding paragraph has been rewritten and now reads (Line 395-408):

*“However, discrepancies in the ensemble mean fire aerosol SCRE (Fig. 14b) are substantial when the number of ensemble members is small. The same is true for the ensemble spread of fire aerosol SCRE (Fig.S8).In order to quantify the discrepancies of the simulated SCRE, we chose the ensemble mean SCRE in the 20-member simulation as a reference and use the root mean square errors (RMSE) of the ensemble mean SCRE in the N-member simulation to quantify the deviation of the simulated SCRE from the reference value. It is calculated as the standard deviation of the differences between the daily ensemble mean SCRE in the N-member simulation and the 20-member simulation. For each N, we randomly sampled 1000 times from the 20 members to help reduce the influence from limited sampling. Figure 15 shows that both the RMSE of ensemble*



mean SCRE and the difference of RMSE between the 1000 groups of simulations (for each N) decrease with increasing N. The minimum number of N required is determined when the 90<sup>th</sup> percentile of RMSE is smaller than a threshold RMSE. Without a good reference, we set the threshold RMSE to 20% ( $0.566\text{Wm}^{-2}$ ) of the reference 10-day mean SCRE ( $-2.83\text{W m}^{-2}$ ). As shown in Fig.15, at least 11 members are needed to meet this criterion.”

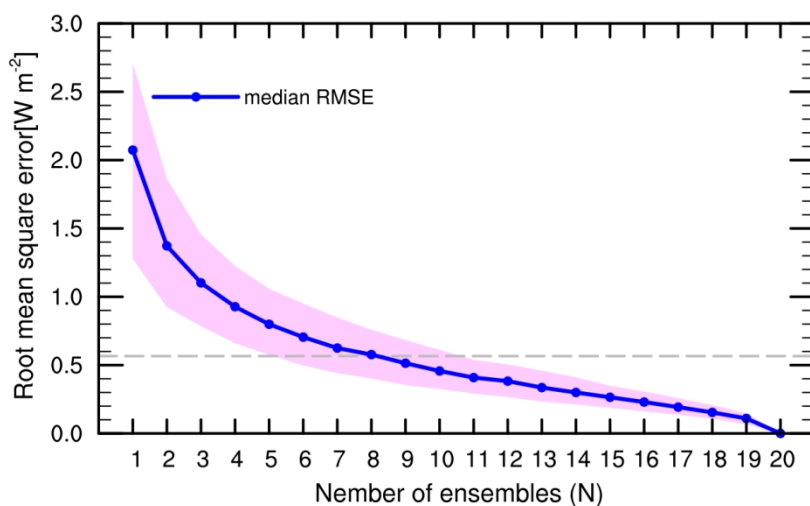


Figure 15 Root mean square errors (RMSE) of the ensemble mean of the regional mean fire aerosol SCRE during April 1-10 over Southern Mexico in simulations with different total number of ensemble members (N). The blue line represents the median RMSE of the 1000 groups (each group has N members/simulations). The grey line represents the threshold RMSE. Shaded area denotes the range between the 10<sup>th</sup> and 90<sup>th</sup> percentiles.

Comment: Fig3: Please give full name of TCC.

Reply: Full name of TCC is temporal correlation coefficient. We now provide the full name in the revised paper.

Comment: Fig7: what is the KS test? Please give full name

Reply: Full name of the KS test is Kolmogorov-Smirnov test. We now provide the full name in the revised paper.

Comment: Fig10: is a) total aerosol direct forcing?

**Reply:** Yes. We have clarified this in the revised paper.

1 **Investigating the short-term effective radiative forcing of fire**  
2 **aerosols using nudged hindcast ensembles**

3 Yawen Liu<sup>1,2</sup>, Kai Zhang<sup>2</sup>, Yun Qian<sup>2</sup>, Yuhang Wang<sup>3</sup>, Yufei Zou<sup>3</sup>, Yongjia Song<sup>3</sup>, Hui Wan<sup>2</sup>,  
4 Xiaohong Liu<sup>4</sup>, and Xiu-Qun Yang<sup>1</sup>

5 <sup>1</sup>School of Atmospheric Sciences, Nanjing University, Nanjing, China

6 <sup>2</sup>Pacific Northwest National Laboratory, Richland, Washington, USA

7 <sup>3</sup>School of Earth and Atmospheric Sciences, Georgia Institute of Technology, Atlanta, Georgia, USA

8 <sup>4</sup>Department of Atmospheric Science, University of Wyoming, Laramie, Wyoming, USA

9

10

11 Corresponding to: Yun Qian [Yun.Qian@pnnl.gov]

12

13

14

15

16

17

18

## 19 **Abstract**

20 Aerosols from fire emissions can potentially have large impact on clouds and radiation. However, fire aerosol sources  
21 are often intermittent and their effect on weather and climate is difficult to quantify. Here we investigated the short-  
22 term effective radiative forcing of fire aerosols using the global aerosol-climate model Community Atmosphere Model  
23 Version 5 (CAM5). Different from previous studies, we used nudged hindcast ensembles to quantify the forcing  
24 uncertainty due to the chaotic response to small perturbations in the atmosphere state. Daily mean emissions from  
25 three fire inventories were used to consider the uncertainty in emission strength and injection heights. The simulated  
26 aerosol optical depth (AOD) and mass concentrations were evaluated against in-situ measurements and re-analysis  
27 data. Overall, the results show the model has reasonably good predicting skills. Short (10-day) nudged ensemble  
28 simulations were then performed with and without fire emissions to estimate the effective radiative forcing. Results  
29 show fire aerosols have large effects on both liquid and ice clouds over the two selected regions in April 2009.  
30 [Ensemble mean results show strong negative shortwave cloud radiative effect \(SCRE\) over almost the entire Southern](#)  
31 [Mexico, with a 10-day regional mean value of  \$-3.02 \text{ W m}^{-2}\$ . Over the Central U.S, the SCRE is positive in the north](#)  
32 [but negative in the south and the regional mean SCRE is small \( \$-0.56 \text{ W m}^{-2}\$ \).](#) For the 10-day average, we found a  
33 large ensemble spread of regional mean shortwave cloud radiative effect over Southern Mexico (15.6% [of the](#)  
34 [corresponding ensemble mean](#)) and the Central U.S. (64.3%), despite that the regional mean AOD time series are  
35 almost indistinguishable during the 10-day period. Moreover, the ensemble spread is much larger when using daily  
36 averages instead of 10-day averages. [For the case investigated here, a minimum of 9 ensemble members is necessary](#)  
37 [to get a reasonable estimate of the ensemble mean and spread of the forcing on individual days.](#) This demonstrates the  
38 importance of using a large ensemble of simulations to estimate the short-term aerosol effective radiative forcing.

## 39 **1. Introduction**

40 Natural and human-induced fires play an important role in the Earth system. Aerosol and gas emissions from biomass  
41 burning can change the atmospheric composition and potentially affect the weather and climate. Over 30% of the  
42 global total emission of black carbon (BC) comes from open burning of forests, grasslands and agricultural residues  
43 (Bond et al. 2013). For organic aerosols, substantial increases of concentrations dominated by organic carbon  
44 enhancements are observed in regions with biomass burning events (Zeng et al. 2011; Lin et al. 2013; Brito et al.  
45 2014; Reddington et al. 2014). As a result, biomass burning emissions have a large impact on the global and regional  
46 mean aerosol optical depth (Jacobson, 2014).

47 Through interactions with radiation and cloud, fire aerosols can significantly affect the long-term Earth's energy  
48 budget. Previous studies have investigated the global and regional radiative forcing of fire aerosols using long  
49 climatological simulations or satellite retrievals. For example, Ward et al. (2012) investigated the radiative forcing of  
50 global fires in pre-industrial, present day, and future periods. For the present-day condition, they estimated a direct  
51 aerosol effect (or radiative forcing through aerosol-radiation interactions as defined in IPCC AR5, RFari; see section  
52 2.4) of  $+0.1 \text{ W m}^{-2}$  and an indirect effect (radiative forcing through aerosol-cloud interactions, RFaci) of  $-1.0 \text{ W m}^{-2}$ .  
53 Using a newer model, Jiang et al. (2016) found similar RFari but slightly smaller RFaci ( $-0.70 \text{ W m}^{-2}$ ). Sena et al.

54 (2013) assessed the direct impact of biomass burning aerosols over the Amazon basin using satellite data. Over the  
55 10-year ~~studied-study~~ period, the estimated radiative forcing is about  $-5.6 \text{ W m}^{-2}$ .

56 On short timescales, fire aerosols have even larger radiative impacts. Observed maximum daily direct aerosol  
57 radiative effects can reach  $-20 \text{ W m}^{-2}$  at TOA locally in Amazonia during biomass burning seasons (Sena et al., 2013).  
58 Very large direct effects of fire aerosols were observed during extreme fire events over Central Russia (Tarasova et  
59 al. 2004; Chubarova et al. 2008; Chubarova et al. 2012). Instantaneous direct radiative effects of emitted aerosols  
60 reached  $-167 \text{ W m}^{-2}$  and monthly mean direct radiative effects reached about  $-65 \text{ W m}^{-2}$  in the 2010 Russia wildfires  
61 (Chubarova et al. 2012). Kolusu et al. (2015) investigated direct radiative effect of biomass burning aerosols over  
62 tropical Southern America. By quantifying results from the first and second day of 2-day single-member forecasts in  
63 September 2012, they found the modeled biomass burning aerosols reduced all-sky net radiation by  $8 \text{ W m}^{-2}$  at TOA  
64 and  $15 \text{ W m}^{-2}$  at surface Fire aerosol indirect effect may also significantly affect the cloud formation and radiative  
65 balance on short time scales. Using satellite data and a radiative transfer model, Kaufman et al. (2005) found an  
66 indirect radiative effect of  $-9.5 \text{ W m}^{-2}$  due to smoke aerosol-induced cloud changes over Southeast Atlantic for the 3  
67 months studied. Smoke-derived cloud albedo effect on local shortwave radiative forcing is estimated to be between -  
68 2 and  $-4 \text{ W m}^{-2}$  in a day case study of aircraft-measured indirect cloud effects (Zamora et al., 2016). ~~Kolusu et al.~~  
69 ~~(2015) investigated direct radiative effect of biomass burning aerosols over tropical Southern America. By quantifying~~  
70 ~~results from the first and second day of 2 day single member forecasts in September 2012, they found the modeled~~  
71 ~~biomass burning aerosols reduced all sky net radiation by  $8 \text{ W m}^{-2}$  at TOA and  $15 \text{ W m}^{-2}$  at surface.~~

72 Previous modeling studies on the short-term fire aerosol effects mainly focused on aerosol direct effects (e.g., Keil  
73 and Haywood, 2003; Chen et al., 2014; Kolusu et al., 2015), and only a couple of studies investigated the indirect  
74 effects of fire aerosols (Lu et al. 2013). In addition, to estimate the aerosol indirect effect, long simulations (multi-  
75 years, >5 years preferred) are often needed to remove the noise, because aerosol life cycle and cloud properties are  
76 affected by strong natural variability on different timescales (Bony et al. 2006; Kooperman et al. 2012). To solve the  
77 problem, alternative methods have been proposed to help extract signals with shorter simulations. For example,  
78 nudging (also called Newton relaxation method) can help reduce uncertainties associated with natural variability by  
79 constraining certain meteorological fields towards prescribed conditions. A robust estimate of global anthropogenic  
80 aerosol indirect effects can be obtained on substantially shorter timescales (1-2 years) by implementing nudging to  
81 constrain simulations with pre-industrial and present-day aerosol emissions toward identical circulation and  
82 meteorology (Kooperman et al. 2012). When nudged towards re-analysis data, Zhang et al. (2014) found constraining  
83 only the horizontal winds is a preferred strategy to estimate the aerosol indirect effect since it provides well-  
84 constrained meteorology without strongly perturbing the model's mean climate state. Another example is the use of  
85 representative ensembles of short simulations to replace a typical long integration. Wan et al. (2014) explored the  
86 feasibility of this method and showed that 3-day ensembles of 20 to 50 members are able to reveal the main signals  
87 revealed by traditional 5-year simulations.

88 In this study, we performed month-long and 10-day nudged CAM5 simulations to investigate the effects of fire  
89 aerosols on radiation and cloud processes on short time scales (less than two weeks). Horizontal winds were nudged  
90 towards 6-hourly reanalysis to constrain the large-scale circulation and to allow for more accurate model evaluations

91 against observations. We also used daily mean emissions from three fire inventories to consider the uncertainty in  
92 emission strength and injection heights. Even for short simulations, small perturbations of meteorological states might  
93 have large impact on the local aerosol and cloud properties, thus bring uncertainty to the aerosol forcing estimate.  
94 Therefore, in our simulations, we also employed very weak temperature nudging ([~10days](#)) in combination with  
95 ensembles to quantify the uncertainty. [More details of the nudging setup are described in section2.3.](#)

96 The rest of the paper is organized as follows. Sect. 2 describes the model and data used in this study. It also  
97 introduces how the ensembles are generated in the short nudged simulations and explains how the fire aerosol forcing  
98 is estimated. Results and discussions are presented in Sect. 3 and conclusions are summarized in Sect. 4

## 99 **2. Model, Method and Data**

### 100 **2.1 Model description**

101 In this study, we used the Community Atmosphere Model (CAM) version 5.3 with the finite volume dynamical core  
102 at  $1.9^\circ$  (latitude)  $\times$   $2.5^\circ$  (longitude) horizontal resolution with 30 vertical layers. The aerosol life cycle is represented  
103 using the modal aerosol module MAM3 (Liu et al., 2012). CAM5 links the simulated aerosol fields with cloud and  
104 radiation through interactions of the aerosol module with the cloud microphysics and radiative transfer  
105 parameterizations. The two-moment bulk cloud microphysics scheme from Morrison and Gettelman (2008) is used to  
106 track mass mixing ratios and number concentrations of cloud droplets and ice crystals in stratiform clouds.  
107 Representation of shallow convection is based on the work of Park and Bretherton (2009). The deep convection  
108 parameterization was developed by Zhang and McFarlane (1995) and later revised by Richter and Rasch (2008) and  
109 Neale et al. (2008). Longwave and shortwave radiative transfer are calculated with the Rapid Radiative Transfer Model  
110 for GCMs (RRTMG, Malwer et al. 1997; Iacono et al. 2008).

### 111 **2.2 Fire Emission Inventories**

112 Three fire emission inventories were used in this study. Two of them are widely used bottom-up inventories— Global  
113 Fire Emissions Database version 3.1 (GFED v3.1, van der Werf et al., 2010; [https://daac.ornl.gov/cgi-  
114 bin/dsviewer.pl?ds\\_id=1191](https://daac.ornl.gov/cgi-bin/dsviewer.pl?ds_id=1191)) and GFED v4.1s (Giglio et al. 2013; Randerson et al. 2012;  
115 [https://daac.ornl.gov/VEGETATION/guides/fire\\_emissions\\_v4.html](https://daac.ornl.gov/VEGETATION/guides/fire_emissions_v4.html)). Another one is a top-down emission  
116 inventory—Quick Fire Emissions Dataset version 2.4 (QFED v2.4). GFED v3.1 and GFED v4.1s provide global  
117 monthly emissions at  $0.25 \times 0.25$  degree spatial resolution from 1997 through the present. Daily emission data [arecan  
118 be](#) obtained by disaggregating monthly emissions based on daily temporal variability in fire emissions derived from  
119 MODIS measurements of active fires (Mu et al. 2011). [The daily emission data is obtained using daily scalars  
120 \(http://www.globalfiredata.org/data.html\) to distribute monthly emissions over the days and is only available from  
121 2003 onwards.](#) The more recent version GFED v4.1s improves by including small fires based on active fire detections  
122 outside the burned area maps (Randerson et al., 2012). QFED v2.4 estimates global fire emissions using the Moderate  
123 Resolution Imaging Spectroradiometer (MODIS) measurements of fire radiative power and generates daily products  
124 at  $0.1 \times 0.1$  degree resolution.

125 To drive CAM5 simulations, fire emission data were regridded to the model resolution and distributed vertically.  
126 For the GFED v3.1 and QFED v2.4 emission data we adopted the same injection heights (from surface to 6 km) as  
127 used in the standard CAM5 model. While for GFEDv4.1s, in this study the injection heights were estimated using a  
128 fire plume model and scaled to the 6-hourly interval.

129 The fire emission inventories were first analyzed to select appropriate time periods and regions for our study before  
130 being used to drive model simulations. Fig.1 shows the multi-year mean biomass burning emissions from GFED v4.1  
131 over North America. The emission manifests significant seasonality with large dry matter consumption during March  
132 to April and June to September. The summer and autumn burning covers Pacific Northwest and part of Canada and is  
133 mainly associated with forest fires, while the spring burning occurs in more densely populated regions like Mexico  
134 and central and eastern United States with a large contribution of agricultural fires in croplands (Korontzi et al., 2006;  
135 Magi et al., 2012). Similar features are also captured in GFED v3.1 and QFED v2.4 with differences in the magnitude.  
136 We chose to analyze the simulated fire aerosol effect in April, the peak month of spring burning, when there are  
137 extreme fire activities over Mexico (10 N to 25N, 100W to 80W) and occasionally large fires in the Central U.S. (35  
138 N to 45N, 100W to 85W). For the U.S., extended fire period is rare, making it necessary to perform short-term  
139 evaluation. Fire aerosols formed from these two regions are often transported to the Eastern and Southeastern U.S.,  
140 where they mix with aerosols from anthropogenic sources and potentially have significant impact on clouds and  
141 radiation over these areas. Time series of regional mean fire emissions in April during 2003-2014 shows that relatively  
142 large fires occur in both regions in 2009 (Fig.S1). Values of fire emissions in 2009 are larger than the multi-year April  
143 mean by a factor of 1.9 in the Central U.S. and 1.5 in Southern Mexico. Thus, in the following model simulations, we  
144 focused on analyzing the aerosol properties and radiative effects over the two selected regions (denoted by the red  
145 boxes in Fig.1) in April, 2009.

146 Fire emitted BC from different emission inventories in April, 2009 is shown in Fig.2. Although GFED v4.1s  
147 includes the contributions of small fires (Randerson et al., 2012), the emitted BC in GFED v4.1 shows no substantial  
148 increase compared to GFED v3.1 during the selected period. Only an increase by 1.75 is seen over Southern Mexico.  
149 In the Central U.S., the BC emission is even slightly weaker in GFED v4.1. QFED v2.4 shows a much larger BC  
150 emission than the GFED inventories. ~~Monthly mean Values~~-values of emitted BC in QFED v2.4 are larger than those  
151 in GFED v4.1s by a factor of ~~9.7-11.4~~ in the Central U.S. and a factor of ~~2.7-3.3~~ in Southern Mexico.

## 152 **2.3 Simulations**

153 Two groups of simulations were conducted (Table1) using the same greenhouse gas concentrations, sea surface  
154 conditions and anthropogenic emissions of aerosols and precursors. Each group includes four simulations, performed  
155 either without fire emission or with daily fire emissions from one of the three fire emission inventories introduced in  
156 section 2.2. The emitted species include BC, OC, and SO<sub>2</sub>. Horizontal winds were nudged to 6-hourly ERA-Interim  
157 reanalysis (Dee et al., 2011) as described in Zhang et al. (2014) in both groups.

158 Simulations in Group A are month-long single-member nudged simulations. These simulations were performed to  
159 provide longer time series for model evaluation and generate initial condition files for simulations in Group B. They

160 started from January 1, 2009 and were integrated for four months with 3-month spin-up. Initial condition files were  
161 generated on April 1 at 00 UTC for simulations in group B.

162 Simulations in group B are 10-day ensemble simulations. Unlike the traditional way of perturbing initial  
163 conditions, in this study we constructed the ensembles by implementing a very weak temperature nudging and  
164 perturbing the nudging time scale. This is because under the influence of horizontal-wind nudging, ensemble  
165 differences generated by perturbing initial conditions would fade away during the integration. In contrast, our method  
166 can consider the influence of small temperature perturbations during the entire simulation period, as nudging is applied  
167 at every time step. On the other hand, the large-scale circulation patterns simulated in the different ensemble members  
168 are very similar (not shown), so the noises caused by the chaotic system can be constrained and the effective fire  
169 aerosol forcing signal can be easily identified.

170 Each ensemble in group B includes 10 members. The only difference between the members is the relaxation time  
171 scale of temperature, which varies from 10 to 11 days at an interval of 0.1 day. All simulations started on April 1,  
172 2009 and were integrated for 10 days. For each simulation (e.g. E\_QF), the initial condition was generated by  
173 combining the meteorological fields from initial condition outputs in the S\_NF simulation with aerosol and precursor  
174 concentrations from initial condition outputs in the single-member simulation forced by the corresponding fire  
175 emission (S\_QF).

## 176 2.4 Calculation of fire aerosol RF

177 The IPCC AR5 report provides a more useful characterization of aerosol forcing by allowing for rapid tropospheric  
178 adjustments (Boucher et al., 2013) compared to the original definition of aerosol forcing. It quantifies aerosol radiative  
179 effects in terms of Effective Radiative Forcing from aerosol-radiation interactions (ERF<sub>ari</sub>) and Effective Radiative  
180 Forcing from aerosol-cloud interactions (ERF<sub>aci</sub>). ERF<sub>ari</sub> refers to the combined effect of instantaneous radiative  
181 forcing from direct scattering and absorption of sunlight (aerosol direct effect) and related subsequent rapid  
182 adjustments of atmospheric state variables and cloudiness (aerosol semi-direct effect). ERF<sub>aci</sub> refers to the indirect  
183 forcing resulting from aerosol induced changes in cloud albedo (first albedo effect) and subsequent changes in cloud  
184 lifetime as rapid adjustments (second aerosol indirect effect) via microphysical interactions.

185 To allow for a straightforward comparison with previous studies in the literature, we followed the IPCC concept  
186 of including rapid adjustments (effective aerosol radiative forcing), but continued to decompose the aerosol effect in  
187 the conventional terms as aerosol direct radiative effect (DRE), aerosol cloud radiative effect (CRE) and surface albedo  
188 effect. Note that as nudging timescale determines the degree to which model physics are constrained (Kooperman et  
189 al., 2012), the use of a 6-hour relaxation time scale for horizontal wind nudging means only very fast adjustments are  
190 considered in the simulations.

191 Similar to Jiang et al. (2016), our calculations ~~of fire aerosol DRE, CRE and surface albedo effect~~ are based on the  
192 work of Ghan et al. (2012) and Ghan (2013). Fire aerosol DRE, CRE and surface albedo effect are defined as fire  
193 induced changes in aerosol forcing, cloud forcing, and surface albedo forcing respectively, and are calculated as the  
194 difference of each item ~~They were calculated as the radiative flux differences~~ between simulations with and without  
195 fire emissions (denoted by  $\Delta$ ). In each simulation, aerosol ~~(direct)~~ forcing was defined as the difference between all-



196 sky and clean-sky TOA radiative fluxes ( $F - F_{\text{clean}}$ ). ~~Aerosol-induced e~~Cloud forcing ~~change~~ was defined as the  
197 difference between all-sky and clear sky TOA radiative fluxes under clean-sky conditions ( $F_{\text{clean}} - F_{\text{clean,clear}}$ ). The  
198 rest were related to surface albedo forcing ( $F_{\text{clean,clear}}$ ). Thus fire aerosol DRE, CRE, and surface albedo effect were  
199 expressed as  $\Delta(F - F_{\text{clean}})$ ,  $\Delta(F_{\text{clean}} - F_{\text{clean,clear}})$ , and  $\Delta F_{\text{clean,clear}}$ , respectively. More details about the method can  
200 be found in section 2 of Ghan (2013). CRE includes contributions of both aerosol indirect effect and aerosol semi-  
201 direct effect but was analyzed as a single term (i.e., the sum).

## 202 2.5 Observational Data

203 In this study, we used two sets of AOD reanalysis and the AERONET data (Holben et al. 1998) to evaluate the  
204 modeled AOD. The two AOD reanalysis datasets are the Naval Research Laboratory (NRL) reanalysis (Rubin et al.  
205 2015) and the Monitoring Atmospheric Composition and Climate (MACC) reanalysis (Eskes et al. 2015). Both are  
206 generated by assimilating AOD retrievals from MODIS (Zhang et al., 2008; Benedetti et al., 2009) with forecast fields.  
207 The NRL reanalysis provides 6-hourly AOD at 1°horizontal resolution. The MACC dataset provides 3-hourly AOD  
208 at 1.125°horizontal resolution. Daily averages in April, 2009 were used for model evaluation in this study. AERONET  
209 retrievals of AOD from April 1 to April 30 in 2009 were used for model evaluation. Two sites are available in the  
210 selected regions: Cart\_Site (36°N, 97°W) and Mexico\_City (19°N, 99°W). LEV 2.0 cloud-screened all points AOD  
211 at 500 nm and 675 nm was used to generate hourly AOD at 550nm, which are the processed data based on a cloud-  
212 screening algorithm (Smirnov et al. 2000).

213 In addition, the simulated BC and primary organic matter (POM) concentrations were compared with observations  
214 from the Interagency Monitoring of Protected Visual Environments (IMPROVE) (Malm et al. 2004). IMPROVE  
215 aerosol data are only available over the Central U.S. A total of fifteen sites were selected and marked in Fig 2, which  
216 include the sites west of 94°W near the source region (asterisks) and sites east of 94°W in the downwind region (dots).  
217 Observed organic carbon concentrations were multiplied by 1.4 for comparison with simulated POM. Detailed  
218 descriptions about the data and sites are available at <http://vista.cira.colostate.edu/improve/>. The IMPROVE network  
219 collect 24-hour aerosol data on every third day. Daily averages during April, 2009 are compared on IMPROVE  
220 observation days only.

## 221 3. Results

222 In this part, the model performance is first evaluated based on the simulations in group A. Next, we present the  
223 simulated short-term effective fire aerosol forcing on 10-day and daily timescales based on the results from group B  
224 simulations. We will demonstrate the importance of using ensemble simulations in estimating the short-term aerosol  
225 effective forcing and give a quantitative estimate of how many ensemble members are needed for the case selected in  
226 this study.

### 227 3.1 Model Evaluation

228 Model simulated AOD are evaluated against the NRL and MACC reanalysis data (Fig. 3). The simulated temporal  
229 variation of regional mean AOD over the central U.S. is consistent with that in the reanalysis, but the magnitudes of  
230 simulated AOD are lower (Fig. 3). A better agreement is found between the model and the NRL data, despite the  
231 horizontal winds in the simulation are nudged towards a reanalysis that is very similar to the data used to derive  
232 MACC. Temporal correlation coefficients (TCC) between the modeled AOD and the NRL reanalysis are 0.87 and  
233 0.82 for S\_QF and S\_GF4 simulations, respectively, but are lower (0.67 and 0.78) between the modeled AOD and the  
234 MACC reanalysis data. The corresponding root mean square errors rise from 0.13 (S\_QF) and 0.1 (S\_GF4) to 0.23  
235 and 0.21. Generally, AOD is underestimated by a factor of 2-4 in all simulations compared to the reanalysis, especially  
236 in simulations with GFED emissions. Previous studies have [found the underestimation of AOD in simulations with](#)  
237 [GFED emissions and](#) suggested the need to scale up GFED emissions by a factor of 1-3 to match the observed AOD  
238 (Tosca et al., 2013). This is consistent with the large negative bias in the simulation S\_GF3 and S\_GF4. [However, a](#)  
239 [much larger scale factor might be needed in this case.](#) Simulated AOD in these two simulations are almost  
240 indistinguishable due to the small difference in the total fire emission in the region.

241 Over Mexico, different simulations produce similar temporal variations in AOD, but the magnitude is smaller in  
242 the GFED simulations. [Fire aerosol-induced AOD increase accounts for 8.1% \(S\\_GF3\), 11.2% \(S\\_GF4\) and 48.8%](#)  
243 [\(S\\_QF\) of the background AOD \(Table S2\).](#) Large discrepancies are found between model results and reanalysis data  
244 during Apr. 17-20. An increase of AOD is captured by both reanalysis datasets, while model results display a decrease  
245 of AOD compared to earlier days in the simulation period. Note that the two sets of reanalysis data also have some  
246 differences occasionally. For example, during Apr. 10-12, NRL data displays an increase of AOD, while MACC data  
247 show the opposite. These discrepancies may partly result from the large internal variability in this tropical region,  
248 where the simulated atmosphere state and its influence on aerosol transport are more likely to disagree between the  
249 model and the reanalysis. Generally speaking, the model forced with different fire emissions is capable of capturing  
250 daily variation of AOD in both regions, especially during Apr. 1-10. This period was selected for further investigation  
251 of the short-term fire aerosol effect.

252 Model simulated AOD are also evaluated against AERONET retrievals (Fig. 4). At Cart Site (36°N, 97°W), with  
253 the QFED emission (S\_QF) the model performs well in simulating both the temporal variation (TCC=0.62) and  
254 magnitude of AOD. Simulations with GFED emissions also reproduce the temporal evolution well (TCC = 0.58 for  
255 S\_GF3 and 0.55 for S\_GF4), but with significantly low bias (mean bias by a factor of 2). The simulated difference in  
256 AOD magnitude is similar to that found by Zhang et al. (2014) over the northern sub-Saharan African. Using the  
257 QFEDv2.4 fire emission, the simulated regional mean AOD is a factor of 1.5 higher than that using the GFEDv3.1  
258 emission in their study. Relatively good performance of S\_QF is also seen over Mexico. The simulated time evolution  
259 agrees well with AERONET retrievals except for small discrepancies (e.g. during Apr.17 -19). A better agreement  
260 with the AERONET retrievals is found for the NRL data than MACC reanalysis at both sites. Consistent with the  
261 evaluation using reanalysis, the simulated temporal evolution of AOD during Apr. 1-10 agrees well with both  
262 reanalysis data and AERONET retrievals in selected regions. This gives us further confidence in choosing this period  
263 for further investigation.

264 The model is further evaluated against the IMPROVE data for BC and POM mass concentrations (Fig. 5). In the  
265 downwind region, the simulated mass concentrations in simulation S\_QF lie within a factor of 2 of the observed values  
266 at most sites. However, the magnitude is generally underestimated in simulations with the GFED emissions (S\_GF3  
267 and S\_GF4), especially in S\_GF3. BC and POM concentrations in the downwind regions are affected by transport of  
268 aerosols from Southern Mexico (Fig. S3). A larger amount of fire emission in Southern Mexico would result in a  
269 higher BC (POM) concentration in the downwind region. This explains the slightly higher concentrations in the  
270 simulation S\_GF4 than S\_GF3, as BC and POM emissions over Southern Mexico are higher in GFED v4.1 due to the  
271 inclusion of small fires (Randerson et al., 2012). The good agreement between S\_QF and observations suggests that  
272 the QFED data have a reasonable total emission rate. However, in the source region, the simulation S\_QF displays  
273 large positive bias with a large majority of the values fall out of the a-factor-of-2 band. Given the reasonable total  
274 emission rate in QFED and a good agreement of AOD with AERONET retrievals at Cart\_site, this might result from  
275 the discrepancies in the vertical distribution the fire emissions. Fire-emitted BC and POM in simulations S\_QF and  
276 S\_GF3 reach maximum values in the lowest level and decrease sharply to the next level, while low-level fire emissions  
277 in S\_GF4 distribute in a more uniform way (Fig. S4). As the sampling was done on the lowest model level at most  
278 sites to compare with the IMPROVE data, this explains the strong overestimation in S\_QF. Although the same impact  
279 from vertical distribution of fire emission also appears in simulation S\_GF3, it is partly offset by its negative bias in  
280 the total emission rate.

## 281 **3.2 10-day Mean Results**

282 Given the good model performance during Apr 1-10, we proceed to analyze the short-term effects of fire aerosols  
283 during this period with nudged ensemble simulations. We define “fire AOD” as the AOD difference between the  
284 simulations with and without fire emissions.

### 285 **3.2.1 Fire Aerosol Distribution**

286 Fig. 6 shows the spatial distributions of 10-day average ensemble mean fire AOD. For reference, the total AOD in  
287 the simulation without fire emissions is shown in Fig. S2. During the period, regional mean AOD increases by 6.4%  
288 (E\_GF3), 6.4% (E\_GF4) and 70.2% (E\_QF) in the central U.S. and 10.4% (E\_GF3), 13.3% (E\_GF4), and 49.6%  
289 (E\_QF) in Southern Mexico when fire emissions are included. In E\_QF, high fire AOD covers almost the entire  
290 selected region and extends further north. Maximum values of fire AOD stay above 0.2 around the Yucatan Peninsula.  
291 Over the Central U.S, significant fire AOD ranging between 0.04 and 0.1 appears in the southwest part of the selected  
292 region. Apart from the significant AOD difference in selected regions, large fire AOD also appears near the eastern  
293 coast as a result of local fire emission and the eastward transport of fire aerosols from both regions. Overall, the  
294 modeled fire AOD is much smaller in simulations with GFED emissions.

### 295 **3.2.2 Fire Aerosol Radiative Effect**

296 As described in Sect. 2.4, fire aerosol radiative effect can be decomposed into three items including fire aerosol  
297 DRE, fire aerosol CRE and fire aerosol surface albedo effect (Table S3). Fig.7 shows the spatial distributions of

298 shortwave direct effect (SDRE) and shortwave cloud radiative effect (SCRE). They are major contributors to the total  
299 fire aerosol forcing in the selected regions. For reference, total aerosol forcing and total shortwave cloud forcing in  
300 the simulation without fire emissions are shown in Fig. S2. The spatial distribution of SDRE and SCRE are similar  
301 for the three cases, but with different magnitudes and statistical significant regions for simulations with QFED and  
302 GFED fire emissions. In the Central U.S., fire aerosol SDRE is negligible in GFED forced simulations due to small  
303 fire AOD. Although the fire AOD is larger in simulation E\_QF, the compensation between warming effect of fire BC  
304 and cooling effect of fire POM still results a weak forcing of about  $-0.1 \text{ W m}^{-2}$ . Over southern Mexico, all simulations  
305 produce significant cooling by fire aerosol SCRE with maximum values three times as large as those of corresponding  
306 SDRE. For both SDRE and SCRE, the largest fire aerosol effects appear in the E\_QF simulation while the E\_GF3  
307 yields the weakest forcing, which is consistent with the modeled fire AOD in these simulations.

308 In the following analysis, we will focus on the results from the E\_QF simulation. Both SDRE and SCRE spread  
309 outside the two selected regions and extend eastward reaching coast regions. A stronger fire aerosol effect is seen in  
310 the Southern Mexico region. Strong SDRE appears over the Yucatan Peninsula where fire AOD peaks (Fig. 6).  
311 Regional mean 10-day average of SDRE and SCRE reach  ~~$-1.66$~~  $-0.86$   $\text{W m}^{-2}$  and  $-3.02 \text{ W m}^{-2}$  respectively. It's  
312 interesting to note that the maximum SCRE tends to center around adjacent Gulf of Mexico rather than the land region.  
313 In the central U.S, despite moderate fire aerosol SDRE, ~~SCRE near fire source region is weaker than  $-4 \text{ W m}^{-2}$ , which~~  
314 ~~is comparable to that in the extended regions a positive SCRE exceeding  $2 \text{ W m}^{-2}$  appears in the north part of the~~  
315 ~~region while a comparable negative SCRE appears in the south part of the region-~~

316 To find out the causes of the fire aerosol SCRE, fire aerosol-induced changes in cloud properties are analyzed.  
317 Given the largely insignificant change in cloud fraction (Fig. 8), the negative fire aerosol SCRE in both regions ~~are~~  
318 is mainly ~~induced by changes associated with increases~~ in liquid water path (LWP) and droplet number  
319 concentrations (CDNC). ~~Changes in ice water path (IWP) and ice crystal number concentration (ICNC) can also~~  
320 ~~significantly affect SCRE, but with an opposite sign and mostly in the central U.S. Fire aerosol SCRE in the central~~  
321 ~~U.S is associated with significant increases in both column integrated droplet number concentration (smaller droplet~~  
322 ~~effective radius) and LWP, indicating important contributions of both the aerosol first and second indirect effects.~~  
323 ~~Increased CDNC enhances cloud albedo by decreasing droplet sizes (Twomey, 1977) and allows more liquid water~~  
324 ~~to accumulate by decreasing precipitation efficiency (Albrecht, 1989; Ghan et al., 2012). Note that although LWP~~  
325 ~~and CDNC over southern Mexico change in a smaller magnitude than those in central U.S., fire aerosol SCRE is~~  
326 ~~stronger over Southern Mexico. This is mainly due to the reductions in IWP and ICNC over the Central U.S. These~~  
327 ~~changes, which possibly caused by fire aerosol induced changes in the circulation (Ten Hoeve et al, 2012), lead to a~~  
328 ~~positive SCRE that partly offsets the negative SCRE caused by changes in warm clouds. The increased CDNC due~~  
329 ~~to an increase of CCN from fire aerosols (Fig. 8) leads to smaller droplet sizes, which in turn increase cloud albedo~~  
330 ~~by enhancing backscattering (Twomey, 1977) and further affect LWP by decreasing precipitation efficiency and~~  
331 ~~allowing more liquid water to accumulate (Albrecht, 1989; Ghan et al., 2012). These changes in warm cloud~~  
332 ~~properties demonstrate important contributions of both aerosol first and second indirect effects to the negative~~  
333 ~~SCRE. Over Southern Mexico, although changes of CDNC and LWP are of comparable magnitudes between Gulf~~  
334 ~~of Mexico and the land region (Fig.8), relative changes of both items are much larger over Gulf of Mexico (Fig.S5)~~

335 [due to the smaller magnitudes of background CDNC and LWP here \(Fig. S6\), which tend to lead to a more sensitive](#)  
336 [response of SCRE. That's why the maximum SCRE over Southern Mexico is more centered around Gulf of Mexico.](#)  
337 [Changes in ice water path \(IWP\) and ice crystal number concentration \(ICNC\) can also significantly affect SCRE,](#)  
338 [but with an opposite sign and mostly in the central U.S. The decreased IWP and ICNC, which are possibly caused](#)  
339 [by fire aerosol-induced changes in the circulation \(Ten Hoeve et al, 2012\) and reduced coarse mode dust aerosol](#)  
340 [concentrations \(Fig.S7\), are responsible for the positive SCRE and the negative longwave cloud radiative effect](#)  
341 [\(Table S3\) in the north part of central U.S. In the south part of central U.S., the reduction of IWP and ICNC also](#)  
342 [results in a positive SCRE, which partly offsets the negative SCRE resulting from changes in warm cloud properties.](#)  
343 [This explains the weaker total negative SCRE in this region compared to the Southern Mexico region despite the](#)  
344 [more substantial increase in CDNC and LWP here.](#) In the northeast of the extended coastal regions, a more  
345 significant change of LWP comparable to that in the central U.S appears, while a more significant change of CDNC  
346 comparable to that in Southern Mexico occurs in the southwest. The combined effect leads to the total fire aerosol  
347 effect in the extended regions.

348 The ensemble method provides another effective way to distinguish fire aerosol radiative effect by comparing the  
349 radiative forcing distribution of ensemble members between simulation with and without fire emission. A significant  
350 difference in the distribution of total aerosol (cloud) forcing indicates a significant fire aerosol direct (cloud) effect.  
351 As shown in Fig. 9, a shift towards stronger magnitude occurs to the total aerosol forcing when fire aerosols are  
352 considered. Simulation E\_QF has a larger percentage of grid cells with SDRE below  $-4.2\text{W m}^{-2}$ , while more grid cells  
353 exceed  $-4.2\text{W m}^{-2}$  in E\_NF, which indicates a significant negative fire aerosol direct effect. [The S](#)ame shift also  
354 appears to the total [shortwave](#) cloud forcing with more grid cells having [shortwave](#) cloud forcing below  $-30\text{W m}^{-2}$  in  
355 the simulation E\_QF. Regional mean total aerosol and [shortwave](#) cloud forcing in southern Mexico become more  
356 negative ( $-0.86$  and  $-3.02\text{W m}^{-2}$ ) with fire aerosols.

357 Fig. 10 illustrates ensemble behavior of 10-day average regional mean total aerosol and cloud forcing from all  
358 simulations as well as resulted fire aerosol SDRE and SCRE. The GFED forced simulations not only resemble in  
359 ensemble mean, but also have small difference in ensemble member distribution. Although members in the E\_QF  
360 simulation capture stronger aerosol forcing, thus stronger fire aerosol SDRE than those in E\_GF3 and E\_GF4, the  
361 ensemble spread (as indicated by the maximum and minimum values) in the three simulations is similar. Moreover,  
362 the E\_QF simulation yields a smaller spread of SCRF compared with the GFED forced simulations despite a stronger  
363 ensemble mean SCRF. In each fire simulation, ensemble mean fire aerosol SCRE has a much larger magnitude than  
364 SDRE. So is the corresponding ensemble spread. Taking results from E\_QF simulation as an example, ensemble  
365 spread of SCRE reaches  $0.47\text{W m}^{-2}$ , accounting for 15.6% of the corresponding ensemble mean, while ensemble  
366 spread of SDRE is  $0.03\text{W m}^{-2}$  accounting for 3.5% of the corresponding ensemble mean.

### 367 3.3 Daily RF

368 The fire aerosol effect is also investigated for individual days. The spatial distributions of SDRF and SCRF on April  
369 7 are shown in Fig 11, when relatively high fire emissions appear in both regions. Negative fire aerosol SDRE appears  
370 in the central U.S. biomass-burning region indicating the dominant role of POM scattering. Fire aerosol SDRE over

371 Southern Mexico shows a contrast of warming effect in land region and cooling effect in adjacent ocean despite similar  
372 aerosol loading in the two regions. However, they do have nearly equal clear-sky BC absorption and POM scattering  
373 (Fig. 12). Difference in low-level cloud distributions between two regions leads to different signs of the simulated all-  
374 sky SDRE. Over land, when clouds appear under elevated aerosol layers, more solar radiation is reflected back to  
375 space and this leads to amplified BC absorption and more positive direct aerosol forcing (Keil and Haywood, 2003;  
376 Zhang et al., 2016; Jiang et al., 2016). In contrast, neither absorption nor scattering changes significantly from clear-  
377 sky to all-sky condition over adjacent areas over the ocean, since the small cloud fraction is small. Same enhanced  
378 absorption of above-cloud aerosols is also found over the west Atlantic Ocean. Fire aerosols produce remarkable  
379 negative SCRE up to  $-16\text{W m}^{-2}$  over Southern Mexico land in response to the increase in CDNC and LWP.

### 380 3.4 Discussion about Simulation Strategy

381 Fig. 13 shows the daily variation of the regional mean total (direct) aerosol forcing and cloud forcing. Both the  
382 ensemble mean and spread are investigated here. The total aerosol forcing exhibits considerable diversity across  
383 ensemble members within each simulation even though the simulated AOD is nearly indistinguishable (Fig. 3). Taking  
384 results from simulation E\_QF as an example, maximum values of difference between members exceed  $0.4\text{W m}^{-2}$  for  
385 aerosol forcing and  $5\text{W m}^{-2}$  for cloud forcing, which are approximate 10% of the corresponding ensemble mean values.  
386 The large spread of total aerosol forcing and cloud forcing will lead to uncertainties in the estimation of fire aerosol  
387 effect. This points out the importance of conducting ensemble simulations in order to get a more comprehensive  
388 estimate of daily fire aerosol effect. The minimum ensemble size required for this case is investigated in terms of the  
389 ensemble mean and spread estimate. Simulated ensemble mean fire aerosol SDRE remains nearly unchanged  
390 regardless of the ensemble size (Fig. 14a). However, discrepancies in the ensemble mean fire aerosol SCRF (Fig. 14b)  
391 are substantial when the number of ensemble members is smaller than 8. The same is true for the ensemble spread of  
392 fire aerosol SCRF (Fig. S85). Overall, the time evolution and magnitude of ensemble mean and spread tend to  
393 converge when the number of ensemble members reaches about 9 for different days we investigated here. In order to  
394 quantify the discrepancies of the simulated SCRE, we chose the ensemble mean SCRE in the 20-member simulation  
395 as a reference and use the root mean square errors (RMSE) of the ensemble mean SCRE in the N-member simulation  
396 to quantify the deviation of the simulated SCRE from the reference value. It is calculated as the standard deviation of  
397 the differences between the daily ensemble mean SCRE in the N-member simulation and the 20-member simulation.  
398 For each N, we randomly sampled 1000 times from the 20 members to help reduce the influence from limited  
399 sampling. Figure 15 shows that both the RMSE of ensemble mean SCRE and the difference of RMSE between the  
400 1000 groups of simulations (for each N) decrease with increasing N. The minimum number of N required is determined  
401 when the 90<sup>th</sup> percentile of RMSE is smaller than a threshold RMSE. Without a good reference, we set the threshold  
402 RMSE to 20% ( $0.566\text{Wm}^{-2}$ ) of the reference 10-day mean SCRE ( $-2.83\text{Wm}^{-2}$ ). As shown in Fig.15, at least 11  
403 members are needed to meet this criterion.

404 Fire aerosol sources are often intermittent and height-dependent and there is a need to estimate the short-term  
405 effective aerosol forcing. Although nudging helps to constrain large-scale features, the simulated cloud properties (e.g.  
406 cloud fraction and LWP) and their response to aerosol changes can still be sensitive to small perturbations in the

407 atmospheric state. Therefore, for investigating the short-term aerosol effect, a single simulation might not be sufficient  
408 to tell whether the aerosol effect is significant. The use of ensembles provides an effective way to estimate the  
409 uncertainty. Previous investigations of short-term fire aerosol effect are mainly based on single-member simulations  
410 (Wu et al., 2011; Sena et al., 2013; Kolusu et al., 2015). While this might be less a problem for SDRE, one should be  
411 more careful when investigating the aerosol indirect effect and conduct ensemble simulations to see whether the  
412 estimated fire aerosol effects are robust.

#### 413 **4. Summary**

414 In this study, we investigated the short-term effect of fire aerosols on cloud and radiation using CAM5 simulations.  
415 Month-long single-member simulations and 10-day ensemble simulations were conducted in April, 2009. In order to  
416 help extract signals on short time scales, we used nudging to constrain horizontal winds in all simulations. Our  
417 investigation focused on Southern Mexico where there were constant intensive fire activities and the Central U.S. with  
418 occasionally large fires. Apart from the local effect, fire emissions from the two regions are shown to affect downwind  
419 coastal regions through transport.

420 Modeled AOD and mass concentrations (BC and POM) were evaluated against observations. In general, all  
421 simulations with fire emissions reproduce the observed temporal variation of daily mean AOD well, although the  
422 simulated magnitude is smaller. The model performance is better when QFEDv2.4 is used, which has larger fire  
423 emissions. Modeled regional mean AOD values in simulations using two versions of GFED fire emission data are  
424 barely distinguishable, despite the inclusion of small fires and changed injection heights in GFEDv4.1 used in this  
425 study. Both ~~of them~~ simulate about a factor of 1.5 smaller AOD than that in the simulation using the QFED fire  
426 emissions. At sites in the downwind region, the modeled BC and POM mass concentrations in the simulation with  
427 QFEDv2.4 emission (S\_QF) agree well with the IMPROVE data. In contrast, simulations with the other two fire  
428 emission datasets (S\_GF3 and S\_GF4) have a low bias. The simulated AOD in the source region in S\_QF also agrees  
429 well with the AERONET data (Cart\_Site). If there is no large compensating error in the model, QFEDv2.4 seems  
430 more reasonable in terms of the total (vertically-integrated) emission rate. On the other hand, S\_QF strongly  
431 overestimates BC and POM concentrations in the source region. Considering that the source-region AOD and the  
432 downwind surface mass concentrations are well simulated, the overestimation suggests the actual emission peak might  
433 appear at higher levels compared to the height-dependent injection rates applied in the S\_QF simulation.

434 Based on the evaluation, we chose the first 10 days as the simulation period and focused on the simulation with  
435 QFEDv2.4 fire emission in our ensemble nudged simulations. In our method, the nudged ensembles are generated by  
436 adding a very weak temperature nudging along with horizontal-wind nudging and perturbing the nudging time scale  
437 of temperature gently. In this way, small temperature perturbations are added to the simulation at each time step, while  
438 the large-scale circulation features are very similar between individual members. We first investigated the 10-day  
439 mean effective fire aerosol forcing. Decomposition of total aerosol radiative forcing shows that fire aerosol effects in  
440 the two selected regions are dominated by the ~~shortwave-cloud-radiative-effect~~ SCRE. All fire simulations show  
441 similar spatial distribution of SDRE and SCRE, but with different magnitudes and statistically significant regions. The  
442 similarity in the spatial distribution is expected since the three emission datasets differ mainly in the emission

443 magnitude and no much in spatial distribution in the focus regions of this study. Fire aerosol effects in simulations  
444 with GFED emissions (E\_GF3 and E\_GF4) are weaker than that with QFEDv2.4 emission (E\_QF) by a factor of 1.5  
445 for SCRE and a factor of more than 4 for SDRE. ~~Generally speaking, Overall,~~ the difference in simulated AOD and  
446 fire aerosol indirect radiative effects between simulations is smaller compared to the difference between fire emissions,  
447 consistent with the findings in sub-Saharan African biomass-burning region (Zhang et al. 2014).

448 Fire aerosols produce a negative direct effect of  $-0.1 \text{ W m}^{-2}$  in the Central U.S. and  $-0.86 \text{ W m}^{-2}$  in Southern  
449 Mexico in E\_QF during the 10-day period. Within each region, negative fire aerosol SDRE peaks where fire AOD  
450 reaches maximum. Unlike the limited area affected by significant fire aerosol SDRE, fire aerosol SCRE from selected  
451 regions spreads eastward and northward, affecting remote coast regions. Ensemble mean results show strong SCRE  
452 over almost the entire Southern Mexico, with a 10-day regional mean value of  $-3.02 \text{ W m}^{-2}$ . Over the central U.S, the  
453 SCRE is positive in the north and negative in the south and the regional mean is small ( $-0.56 \text{ W m}^{-2}$ ). Maximum  
454 SCRE stays below  $-4 \text{ W m}^{-2}$  in the (south) central U.S. and  $-10 \text{ W m}^{-2}$  in Southern Mexico in response to  
455 significantly increased LWP and CDNC. Decreases of IWP and ICNC also contribute to fire aerosol SCRE in the  
456 Central U.S. but with an opposite sign. The offset effect of the positive forcing induced by changes in cloud ice  
457 properties explains the smaller SCRE in the central U.S. despite the larger changes in cloud droplet properties.

458 We also investigated fire aerosol effects on the daily time scale, where the variation in the simulated fire aerosol  
459 effect can be large among the ensemble members. The large ensemble spread of total aerosol and cloud forcing  
460 indicates large uncertainties in estimating daily fire aerosol effects, despite similar AOD across ensemble members.  
461 Further investigations show that the simulated ensemble mean and spread with less than 7 members differs  
462 considerably to those with more members. ~~A minimum of 9 members is necessary to achieve a steady estimate of the~~  
463 ~~magnitude and temporal variation of SCRE in this case.~~ Our results suggest that for short-term simulations of aerosol  
464 and cloud processes, even small perturbations might result in large difference across members despite constrained  
465 large scale features. In order to obtain a robust estimate of the effective fire aerosol forcing during a short period, it is  
466 important to conduct ensemble simulations with sufficient ensemble members.

467

468

## 469 Acknowledgments

470 We thank two anonymous reviewers for their careful reviews and suggestions that helped to greatly improve the  
471 analyses and discussion presented in this paper. This study was supported primarily by the U.S. Department of Energy  
472 (DOE)'s office of Science as part of the Regional and Global Climate Modeling Program (NSF-DOE-USDA EaSM2).  
473 The work was also supported by the National Natural Science Foundation of China (NSFC) under Grants No.  
474 41621005 and 41330420, the National Key Basic Research Program (973 Program) of China under Grant No.  
475 2010CB428504, and the Jiangsu Collaborative Innovation Center of Climate. The Pacific Northwest National  
476 Laboratory (PNNL) is operated for DOE by Battelle Memorial Institute under contract DE-AC05-76RL01830.



477 Computations were performed using resources of the National Energy Research Scientific Computing Center  
478 (NERSC) at Lawrence Berkeley National Laboratory and PNNL Institutional computing. All model results are  
479 available from the corresponding author upon request.

480 **References:**

- 481 Albrecht, B. A.: Aerosols, cloud microphysics, and fractional cloudiness, *Science*, 245, 1227-1231, 1989.
- 482 Benedetti, A., Morcrette, J. J., Boucher, O., Dethof, A., Engelen, R., Fisher, M., Flentje, H., Huneeus, N., Jones, L.,  
483 and Kaiser, J.: Aerosol analysis and forecast in the European centre for medium-range weather forecasts integrated  
484 forecast system: 2. Data assimilation, *Journal of Geophysical Research: Atmospheres*, 114, 2009.
- 485 Bond, T. C., Doherty, S. J., Fahey, D., Forster, P., Berntsen, T., DeAngelo, B., Flanner, M., Ghan, S., Kärcher, B.,  
486 and Koch, D.: Bounding the role of black carbon in the climate system: A scientific assessment, *Journal of Geophysical  
487 Research: Atmospheres*, 118, 5380-5552, 2013.
- 488 Bony, S., Colman, R., Kattsov, V. M., Allan, R. P., Bretherton, C. S., Dufresne, J.-L., Hall, A., Hallegatte, S., Holland,  
489 M. M., and Ingram, W.: How well do we understand and evaluate climate change feedback processes?, *Journal of  
490 Climate*, 19, 3445-3482, 2006.
- 491 Boucher, O., Randall, D., Artaxo, P., Bretherton, C., Feingold, G., Forster, P., Kerminen, V.-M., Kondo, Y., Liao, H.,  
492 and Lohmann, U.: Clouds and aerosols, in: *Climate change 2013: the physical science basis. Contribution of Working  
493 Group I to the Fifth Assessment Report of the Intergovernmental Panel on Climate Change*, Cambridge University  
494 Press, 571-657, 2013.
- 495 Brito, J., Rizzo, L. V., Morgan, W. T., Coe, H., Johnson, B., Haywood, J., Longo, K., Freitas, S., Andreae, M. O., and  
496 Artaxo, P.: Ground-based aerosol characterization during the South American Biomass Burning Analysis (SAMBBA)  
497 field experiment, *Atmospheric Chemistry and Physics*, 14, 12069-12083, 2014.
- 498 Chen, D., Liu, Z., Schwartz, C. S., Lin, H.-C., Cetola, J. D., Gu, Y., and Xue, L.: The impact of aerosol optical depth  
499 assimilation on aerosol forecasts and radiative effects during a wild fire event over the United States, *Geoscientific  
500 Model Development*, 7, 2709-2715, 2014.
- 501 Chubarova, N., Nezval, Y., Sviridenkov, I., Smirnov, A., and Slutsker, I.: Smoke aerosol and its radiative effects  
502 during extreme fire event over Central Russia in summer 2010, *Atmospheric Measurement Techniques*, 5, 557-568,  
503 2012.
- 504 Chubarova, N. Y., Prilepsky, N. G., Rublev, A. N., and Riebau, A. R.: A Mega-Fire event in central Russia: fire  
505 weather, radiative, and optical properties of the atmosphere, and consequences for subboreal forest plants,  
506 *Developments in environmental science*, 8, 247-264, 2008.
- 507 Dee, D., Uppala, S., Simmons, A., Berrisford, P., Poli, P., Kobayashi, S., Andrae, U., Balmaseda, M., Balsamo, G.,  
508 and Bauer, P.: The ERA-Interim reanalysis: Configuration and performance of the data assimilation system, *Quarterly  
509 Journal of the royal meteorological society*, 137, 553-597, 2011.
- 510 Eskes, H., Huijnen, V., Arola, A., Benedictow, A., Blechschmidt, A.-M., Botek, E., Boucher, O., Bouarar, I.,  
511 Chabrilat, S., and Cuevas, E.: Validation of reactive gases and aerosols in the MACC global analysis and forecast  
512 system, *Geoscientific model development*, 8, 3523-3543, 2015.

513 Ghan, S. J., Liu, X., Easter, R. C., Zaveri, R., Rasch, P. J., Yoon, J.-H., and Eaton, B.: Toward a minimal representation  
514 of aerosols in climate models: Comparative decomposition of aerosol direct, semidirect, and indirect radiative forcing,  
515 *Journal of Climate*, 25, 6461-6476, 2012.

516 Ghan, S. J.: Technical Note: Estimating aerosol effects on cloud radiative forcing, *Atmos. Chem. Phys.*, 13, 9971-  
517 9974, doi:10.5194/acp-13-9971-2013, 2013.

518 Giglio, L., Randerson, J. T., and van der Werf, G. R. (2013), Analysis of daily, monthly, and annual burned area using  
519 the fourth-generation global fire emissions database (GFED4) *J. Geophys. Res. Biogeosci.*, 118, 317–328,  
520 doi:10.1002/jgrg.20042.

521 Holben, B. N., Eck, T., Slutsker, I., Tanre, D., Buis, J., Setzer, A., Vermote, E., Reagan, J., Kaufman, Y., and  
522 Nakajima, T.: AERONET—A federated instrument network and data archive for aerosol characterization, *Remote  
523 sensing of environment*, 66, 1-16, 1998.

524 Iacono, M. J., Delamere, J. S., Mlawer, E. J., Shephard, M. W., Clough, S. A., and Collins, W. D.: Radiative forcing  
525 by long-lived greenhouse gases: Calculations with the AER radiative transfer models, *Journal of Geophysical  
526 Research: Atmospheres*, 113, 2008.

527 Jacobson, M. Z.: Effects of biomass burning on climate, accounting for heat and moisture fluxes, black and brown  
528 carbon, and cloud absorption effects, *Journal of Geophysical Research: Atmospheres*, 119, 8980-9002, 2014.

529 Jiang, Y., Lu, Z., Liu, X., Qian, Y., Zhang, K., Wang, Y., and Yang, X.-Q.: Impacts of global open-fire aerosols on  
530 direct radiative, cloud and surface-albedo effects simulated with CAM5, *Atmospheric Chemistry and Physics  
531 (Online)*, 16, 2016.

532 Kaufman, Y. J., Koren, I., Remer, L. A., Rosenfeld, D., and Rudich, Y.: The effect of smoke, dust, and pollution  
533 aerosol on shallow cloud development over the Atlantic Ocean, *Proceedings of the National Academy of Sciences of  
534 the United States of America*, 102, 11207-11212, 2005.

535 Keil, A., and Haywood, J. M.: Solar radiative forcing by biomass burning aerosol particles during SAFARI 2000: A  
536 case study based on measured aerosol and cloud properties, *Journal of Geophysical Research: Atmospheres*, 108,  
537 2003.

538 Kolusu, S., Marsham, J., Mulcahy, J., Johnson, B., Dunning, C., Bush, M., and Spracklen, D.: Impacts of Amazonia  
539 biomass burning aerosols assessed from short-range weather forecasts, *Atmospheric Chemistry and Physics*, 15,  
540 12251-12266, 2015.

541 Kooperman, G. J., Pritchard, M. S., Ghan, S. J., Wang, M., Somerville, R. C., and Russell, L. M.: Constraining the  
542 influence of natural variability to improve estimates of global aerosol indirect effects in a nudged version of the  
543 Community Atmosphere Model 5, *Journal of Geophysical Research: Atmospheres*, 117, 2012.

544 Korontzi, S., McCarty, J., Loboda, T., Kumar, S., and Justice, C.: Global distribution of agricultural fires in croplands  
545 from 3 years of Moderate Resolution Imaging Spectroradiometer (MODIS) data, *Global Biogeochemical Cycles*, 20,  
546 2006.

547 Lin, N.-H., Tsay, S.-C., Maring, H. B., Yen, M.-C., Sheu, G.-R., Wang, S.-H., Chi, K. H., Chuang, M.-T., Ou-Yang,  
548 C.-F., and Fu, J. S.: An overview of regional experiments on biomass burning aerosols and related pollutants in  
549 Southeast Asia: From BASE-ASIA and the Dongsha Experiment to 7-SEAS, *Atmospheric Environment*, 78, 1-19,  
550 2013.

551 Liu, X., Easter, R. C., Ghan, S. J., Zaveri, R., Rasch, P., Shi, X., Lamarque, J.-F., Gettelman, A., Morrison, H., and  
552 Vitt, F.: Toward a minimal representation of aerosols in climate models: Description and evaluation in the Community  
553 Atmosphere Model CAM5, *Geoscientific Model Development*, 5, 709, 2012.

554 Liu, X.: Impacts of global open-fire aerosols on direct radiative, cloud and surface-albedo effects simulated with  
555 CAM5, *Atmos. Chem. Phys.*, 1680, 7324, 2016.

556 Lu, Z., and Sokolik, I. N.: The effect of smoke emission amount on changes in cloud properties and precipitation: A  
557 case study of Canadian boreal wildfires of 2007, *Journal of Geophysical Research: Atmospheres*, 118, 2013.

558 Magi, B., Rabin, S., Shevliakova, E., and Pacala, S.: Separating agricultural and non-agricultural fire seasonality at  
559 regional scales, *Biogeosciences*, 9, 3003, 2012.

560 Malm, W. C., Schichtel, B. A., Pitchford, M. L., Ashbaugh, L. L., and Eldred, R. A.: Spatial and monthly trends in  
561 speciated fine particle concentration in the United States, *Journal of Geophysical Research: Atmospheres*, 109, 2004.

562 Mlawer, E. J., Taubman, S. J., Brown, P. D., Iacono, M. J., and Clough, S. A.: Radiative transfer for inhomogeneous  
563 atmospheres: RRTM, a validated correlated-k model for the longwave, *Journal of Geophysical Research:*  
564 *Atmospheres*, 102, 16663-16682, 1997.

565 Morrison, H., and Gettelman, A.: A new two-moment bulk stratiform cloud microphysics scheme in the Community  
566 Atmosphere Model, version 3 (CAM3). Part I: Description and numerical tests, *Journal of Climate*, 21, 3642-3659,  
567 2008.

568 Mu, M., Randerson, J., van der Werf, G., Giglio, L., Kasibhatla, P., Morton, D., Collatz, G., DeFries, R., Hyer, E.,  
569 and Prins, E.: Daily and hourly variability in global fire emissions and consequences for atmospheric model  
570 predictions of carbon monoxide, 2011.

571 Neale, R. B., Richter, J. H., and Jochum, M.: The impact of convection on ENSO: From a delayed oscillator to a series  
572 of events, *Journal of Climate*, 21, 5904-5924, 2008.

573 Park, S., and Bretherton, C. S.: The University of Washington shallow convection and moist turbulence schemes and  
574 their impact on climate simulations with the Community Atmosphere Model, *Journal of Climate*, 22, 3449-3469, 2009.

575 Randerson, J., Chen, Y., Werf, G., Rogers, B., and Morton, D.: Global burned area and biomass burning emissions  
576 from small fires, *Journal of Geophysical Research: Biogeosciences*, 117, 2012.

577 Reddington, C., Yoshioka, M., Balasubramanian, R., Ridley, D., Toh, Y., Arnold, S., and Spracklen, D.: Contribution  
578 of vegetation and peat fires to particulate air pollution in Southeast Asia, *Environmental Research Letters*, 9, 094006,  
579 2014.

580 Richter, J. H., and Rasch, P. J.: Effects of convective momentum transport on the atmospheric circulation in the  
581 Community Atmosphere Model, version 3, *Journal of Climate*, 21, 1487-1499, 2008.

582 Rubin, J. I., Reid, J. S., Hansen, J. A., Anderson, J. L., Hoar, T. J., Reynolds, C. A., Sessions, W. R., and Westphal,  
583 D. L.: Development of the Ensemble Navy Aerosol Analysis Prediction System (ENAAPS) and its application of the  
584 Data Assimilation Research Testbed (DART) in support of aerosol forecasting, *Atmospheric Chemistry and Physics*,  
585 16, 3927, 2016.

586 Sena, E., Artaxo, P., and Correia, A.: Spatial variability of the direct radiative forcing of biomass burning aerosols and  
587 the effects of land use change in Amazonia, *Atmospheric Chemistry and Physics*, 13, 1261-1275, 2013.

588 [Smirnov, A., Holben, B., Eck, T., Dubovik, O., and Slutsker, I.: Cloud-screening and quality control algorithms for](#)  
589 [the AERONET database, \*Remote Sensing of Environment\*, 73, 337-349, 2000.](#)  
590

591 Stier, P., Schutgens, N., Bellouin, N., Bian, H., Boucher, O., Chin, M., Ghan, S., Huneeus, N., Kinne, S., and Lin, G.:  
592 Host model uncertainties in aerosol radiative forcing estimates: results from the AeroCom Prescribed intercomparison  
593 study, *Atmospheric Chemistry and Physics*, 13, 3245-3270, 2013.

594 Tarasova, T., Gorchakova, I., Sviridenkov, M., Anikin, P., and Romashova, E.: Estimation of the radiative forcing of  
595 smoke aerosol from radiation measurements at the Zvenigorod scientific station in the summer of 2002, *Izvestiya*  
596 *Atmospheric and Oceanic Physics*, 40, 454-463, 2004.

597 (Dee et al., 2011), J. E., Jacobson, M. Z., and Remer, L. A.: Comparing results from a physical model with satellite  
598 and in situ observations to determine whether biomass burning aerosols over the Amazon brighten or burn off clouds,  
599 *Journal of Geophysical Research: Atmospheres*, 117, 2012.

600 Tosca, M., Randerson, J., and Zender, C.: Global impact of smoke aerosols from landscape fires on climate and the  
601 Hadley circulation, *Atmospheric Chemistry and Physics*, 13, 5227-5241, 2013.

602 Twomey, S.: The influence of pollution on the shortwave albedo of clouds, *Journal of the atmospheric sciences*, 34,  
603 1149-1152, 1977.

604 van der Werf, G. R., Randerson, J. T., Giglio, L., Collatz, G. J., Mu, M., Kasibhatla, P. S., Morton, D. C., DeFries, R.  
605 S., Jin, Y., and van Leeuwen, T. T.: Global fire emissions and the contribution of deforestation, savanna, forest,  
606 agricultural, and peat fires (1997–2009), *Atmos. Chem. Phys.*, 10, 11707-11735, doi:10.5194/acp-10-11707-2010,  
607 2010.

608 Ward, D., Kloster, S., Mahowald, N., Rogers, B., Randerson, J., and Hess, P.: The changing radiative forcing of fires:  
609 global model estimates for past, present and future, *Atmospheric Chemistry and Physics*, 12, 2012.

610 Wan, H., Rasch, P. J., Zhang, K., Qian, Y., Yan, H., and Zhao, C.: Short ensembles: an efficient method for discerning  
611 climate-relevant sensitivities in atmospheric general circulation models, *Geoscientific Model Development*, 7, 1961-  
612 1977, 2014.

613 Wu, L., Su, H., and Jiang, J. H.: Regional simulations of deep convection and biomass burning over South America:  
614 2. Biomass burning aerosol effects on clouds and precipitation, *Journal of Geophysical Research: Atmospheres*, 116,  
615 2011.

616 Zamora, L. M., Kahn, R., Cubison, M. J., Diskin, G., Jimenez, J., Kondo, Y., McFarquhar, G., Nenes, A., Thornhill,  
617 K., and Wisthaler, A.: Aircraft-measured indirect cloud effects from biomass burning smoke in the Arctic and  
618 subarctic, *Atmospheric Chemistry and Physics*, 16, 715-738, 2016.

619 Zhang, F., Wang, J., Ichoku, C., Hyer, E. J., Yang, Z., Ge, C., Su, S., Zhang, X., Kondragunta, S., and Kaiser, J. W.:  
620 Sensitivity of mesoscale modeling of smoke direct radiative effect to the emission inventory: a case study in northern  
621 sub-Saharan African region, *Environmental Research Letters*, 9, 075002, 2014.

622 Zhang, G. J., and McFarlane, N. A.: Sensitivity of climate simulations to the parameterization of cumulus convection  
623 in the Canadian Climate Centre general circulation model, *Atmosphere-ocean*, 33, 407-446, 1995.

Table 1. List of CAM5 simulations.

Name	Fire emission	Simulation period	Member	Nudging
Group A: Single member simulations				
S_NF	No			
S_GF3	GFED v3			
S_GF4	GFED v4.1	January 1- April 30, 2009	1	Horizontal winds (6h)
S_QF	QFED v2.4			
Group B: Ensemble simulations				
E_NF	No			Horizontal winds (6h) and temperature (~10d)*
E_GF3	GFED v3			
E_GF4	GFED v4.1	April 1 - April 10, 2009	10	
E_QF	QFED v2.4			

\* See section 2.3 for details about ensembles

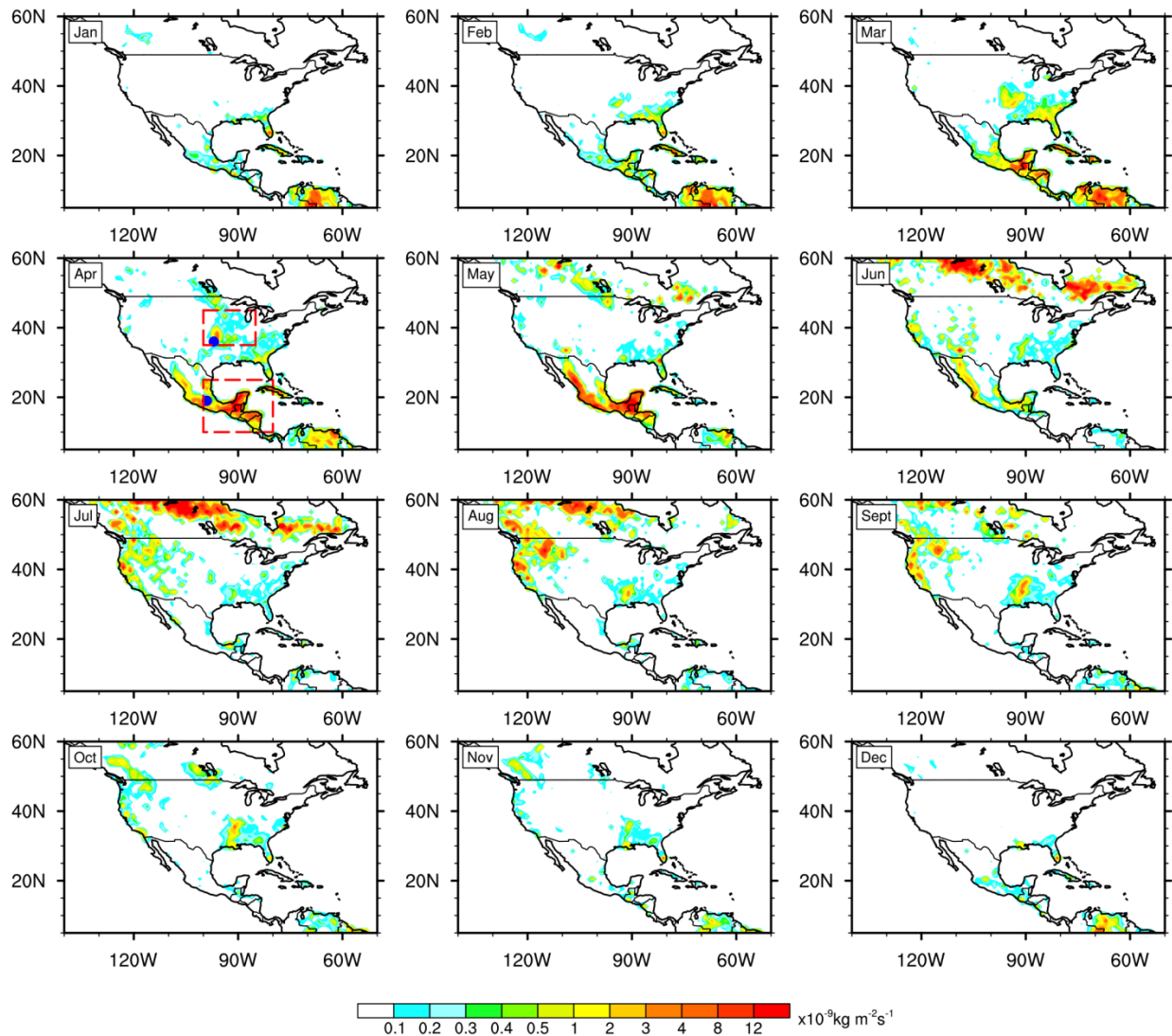


Figure 1. Spatial distributions of multi-year monthly mean biomass burning consumed dry matter over North America during 2003-2014 from GFEDv4.1. Boxes denote selected regions: central U.S. (35 - 45°N, 85 - 100°W) and Southern Mexico (10 - 25°N, 80 - 100°W). Dots denote locations of AERONET sites: Cart\_Site (36°N, 97°W) and Mexico\_City (19°N, 99°W)



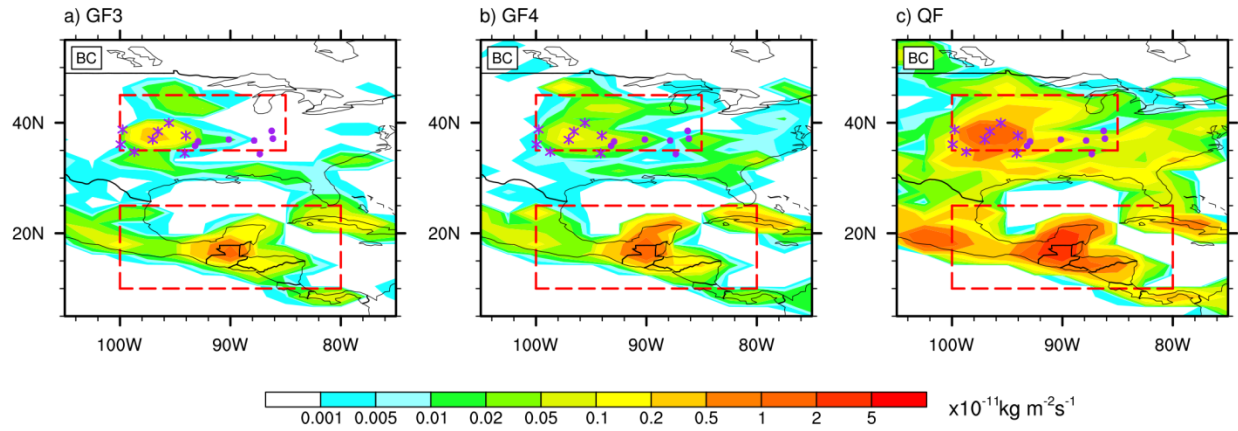


Figure 2. Spatial distributions of monthly mean BC emissions from three emission inventories in April, 2009. IMPROVE data sites are shown as asterisks for sites near the source region and as dots for sites in the region downwind of the fire source.

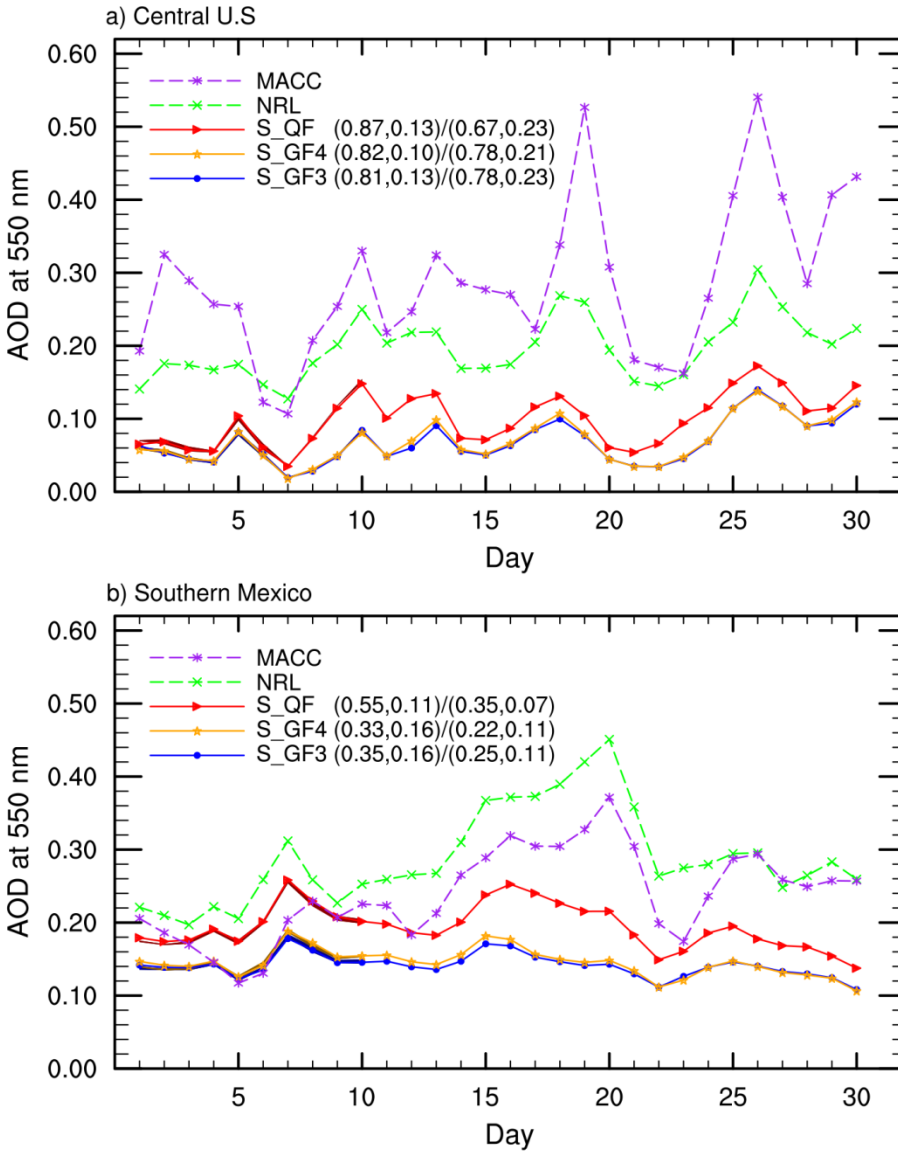


Figure 3. Time series of daily regional mean AOD in April, 2009 in simulations and reanalysis data. Numbers in parenthesis denote [time correlation coefficient \(TCC\)](#) and [root mean square error \(RMSE\)](#) between each simulation in group A and reanalysis data (left: NRL; right: MACC). Individual lines indicate group A simulations. Shaded areas (very narrow) in slightly darker colors during April 1-10 illustrate maximum and minimum values of daily mean AOD among ensemble members in group B simulations. [For the single-member simulation and the ensemble simulation driven by same fire emission, the shaded area and the solid line almost overlap, given the barely indistinguishable AOD between ensemble members and the corresponding Group A simulation.](#)

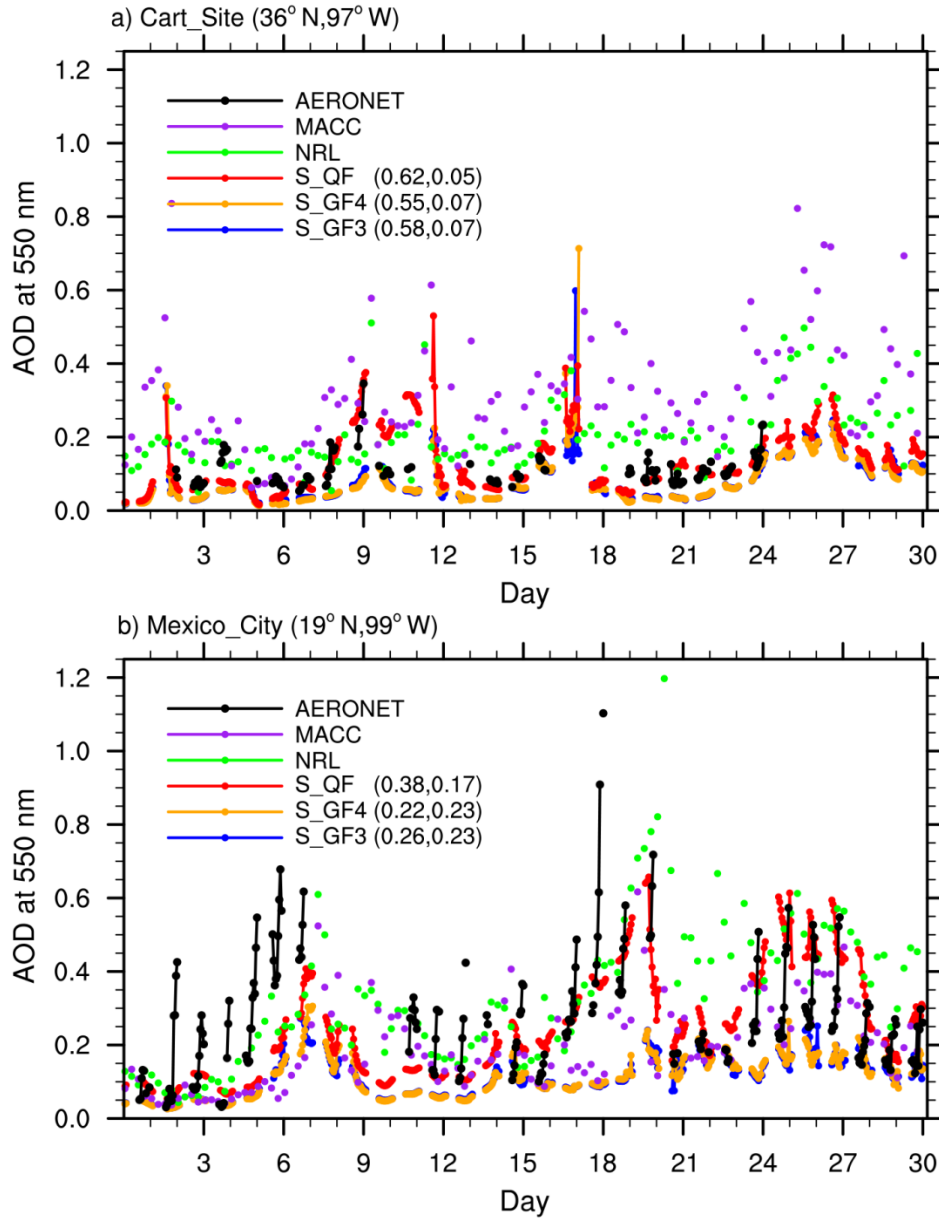


Figure 4. Time series of hourly regional mean AOD in April, 2009 from group A simulations, reanalysis data and AERONET retrievals at AERONET sites. Numbers in parenthesis denote TCC (left) and RMSE (right) between each simulation and AERONET AOD.

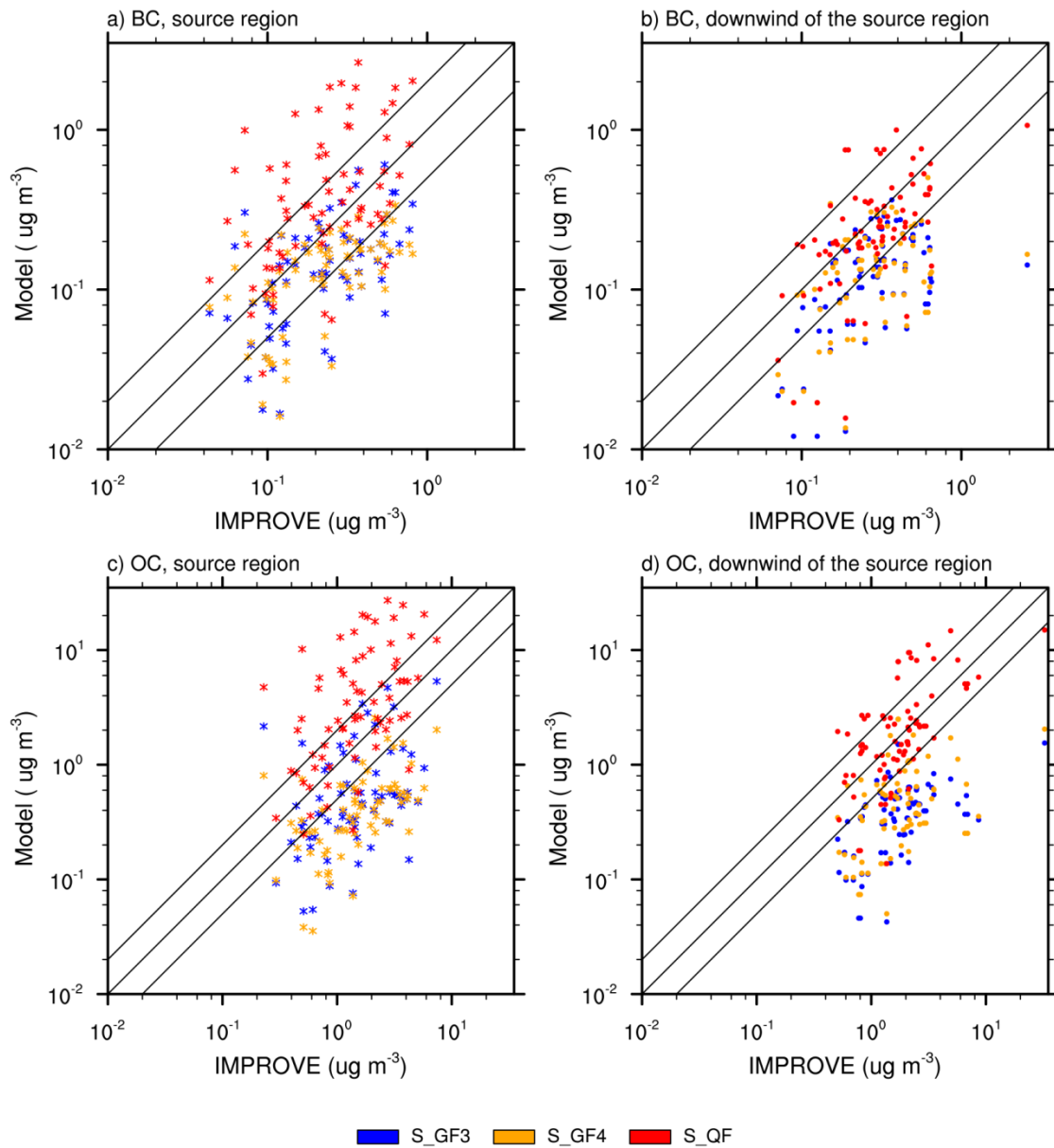


Figure 5. Evaluation of simulated BC (up) and POM (bottom) concentrations in group A simulations against the IMPROVE data at sites near the source and downwind the source region. Locations of these sites are marked with the same symbol in Fig. 2.

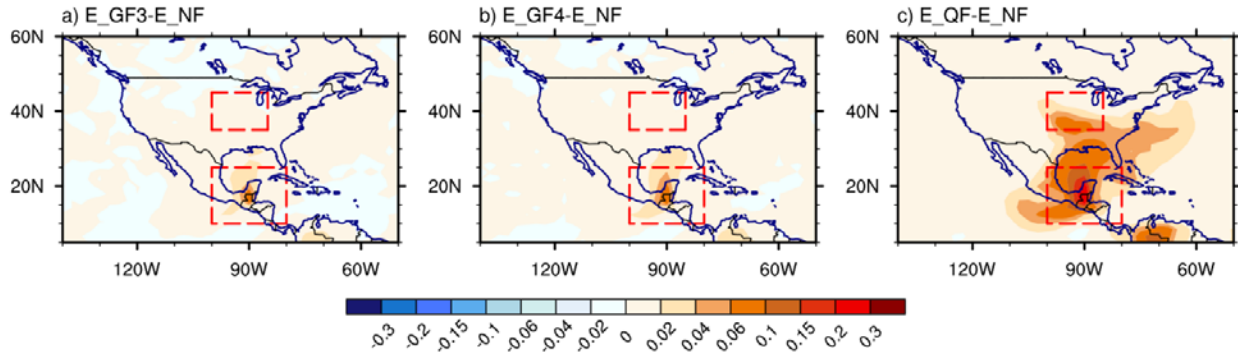


Figure 6. Spatial distributions of 10-day average (Apr. 1-10) ensemble mean AOD differences between simulations with (E\_GF3, E\_GF4, and E\_QF) and without fire emission (E\_NF).

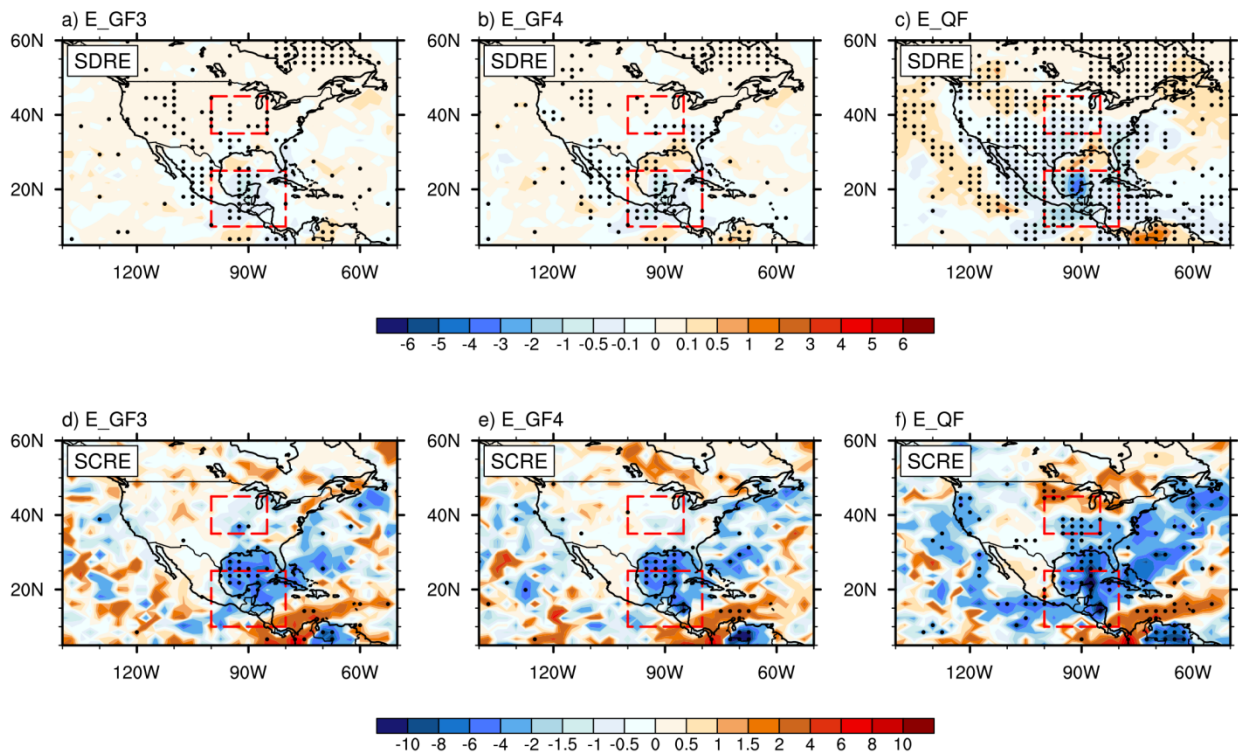


Figure 7. Spatial distributions of 10-day average (Apr. 1-10) ensemble mean fire aerosol shortwave direct radiative effect (SDRE) and shortwave cloud radiative effect (SCRE) ( $W m^{-2}$ ) in group B simulations. Dots denote regions where SDRE is statistically significant at the 95% confidence level based on the [Kolmogorov-Smirnov \(KS\)](#) test.

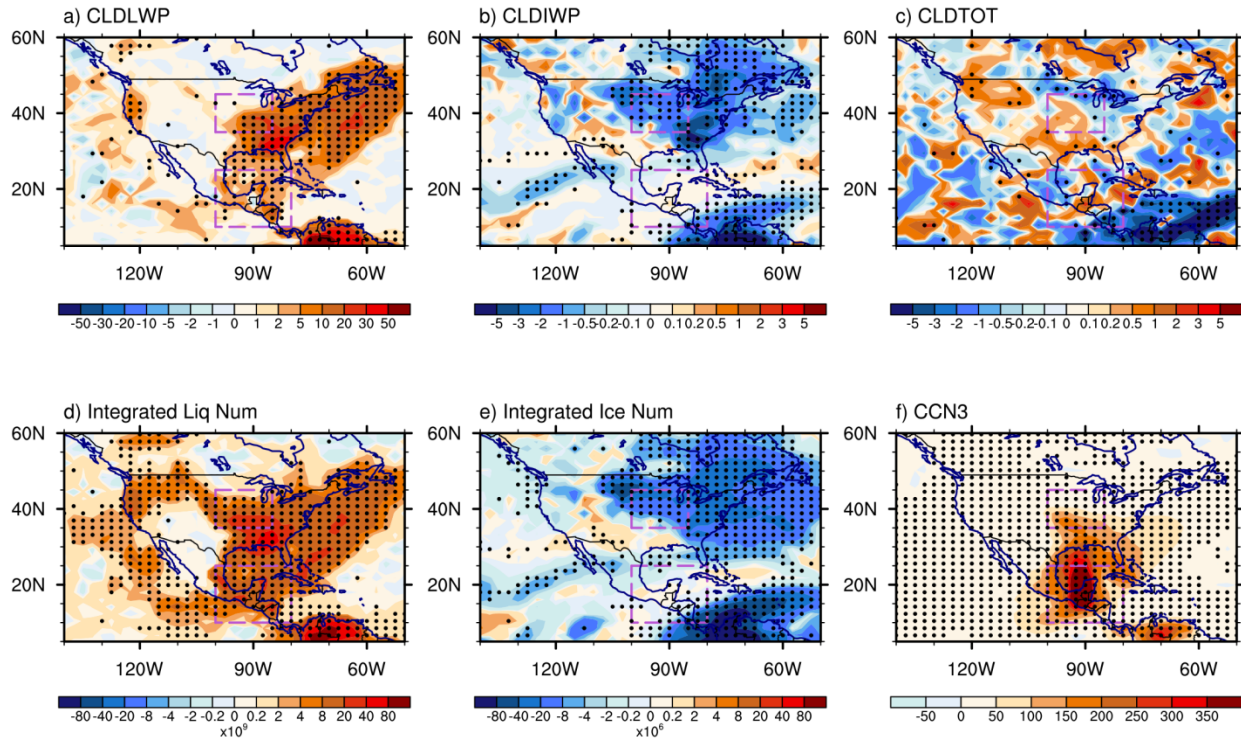


Figure 8. Difference of 10-day average (Apr.1-10) ensemble mean between simulations E\_NF and E\_QF: a) cloud liquid water path (  $\text{g m}^{-2}$  ), b) cloud ice water path (  $\text{g m}^{-2}$  ), c) total cloud fraction (%), d) column-integrated droplet number concentration (  $\text{m}^{-2}$  ), e) column-integrated ice number concentration (  $\text{m}^{-2}$  ), and f) cloud condensation nuclei at 0.1% supersaturation near 900 hPa. Dots denote regions where the difference is statistically significant at the 95% confidence level based on the KS test.

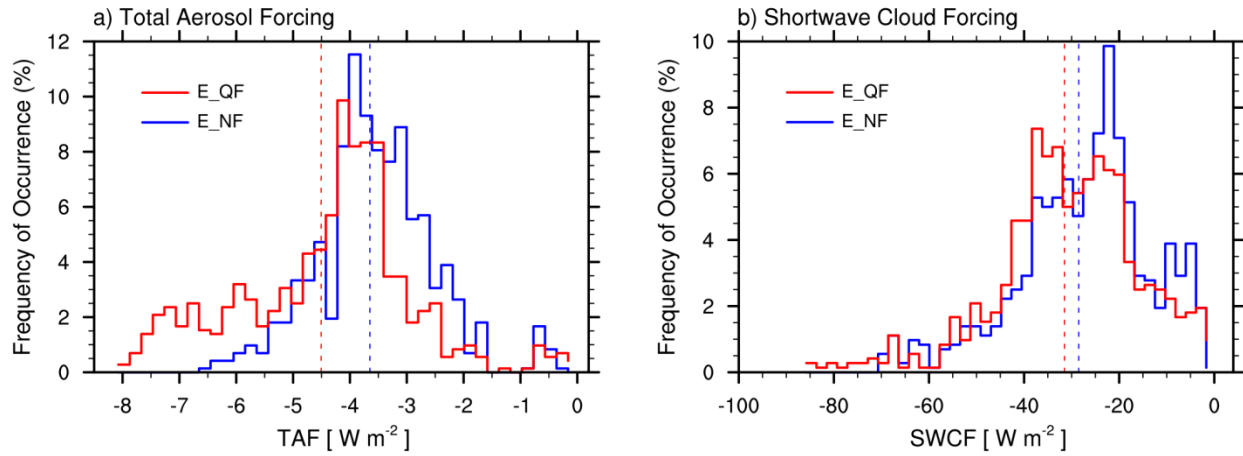


Figure 9. Probability distributions of 10-day average (Apr.1-10) a) total aerosol forcing and b) cloud forcing over Southern Mexico in simulations E\_NF and E\_QF sampled from grid values of ensemble members (72x10 for each case). Dashed lines indicate the mean of the distribution.

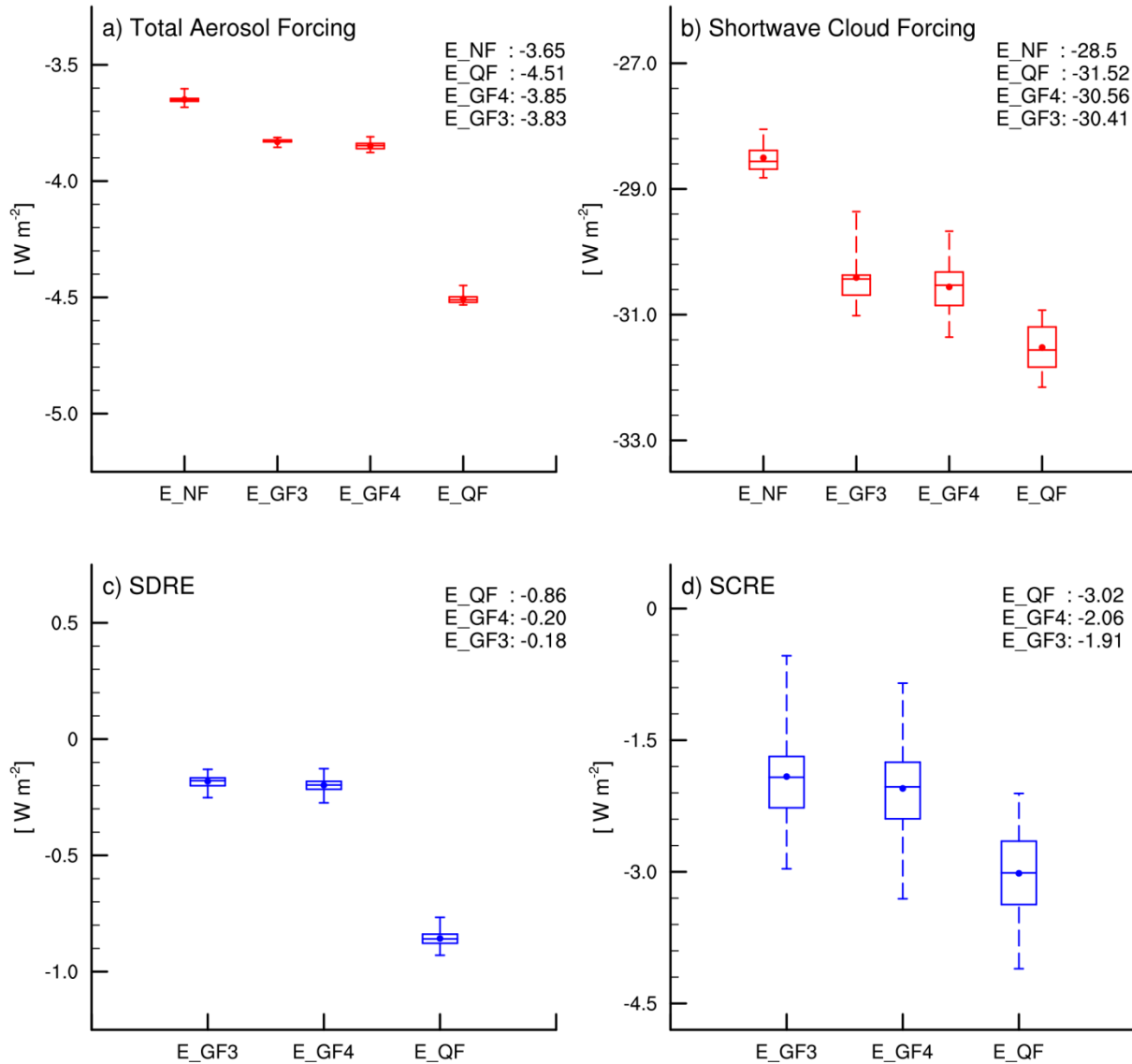


Figure 10. 10-day average (Apr. 1-10) regional mean a) total aerosol [direct](#) forcing, b) total shortwave cloud forcing and fire aerosol, c) SDRE, and d) SCRE in Southern Mexico in group B simulations. Box denotes the 25<sup>th</sup> and 75<sup>th</sup> percentiles. Bars outside the box indicate minimum and maximum. Bar within the box denotes the 50<sup>th</sup> percentile. Total aerosol and cloud forcing are sampled from different ensemble members (10 for each case). Fire aerosol SDRE and SCRF are sampled by calculating the difference between members in simulations E\_QF (E\_GF3/E\_GF4) and E\_NF (10x10 for each case).



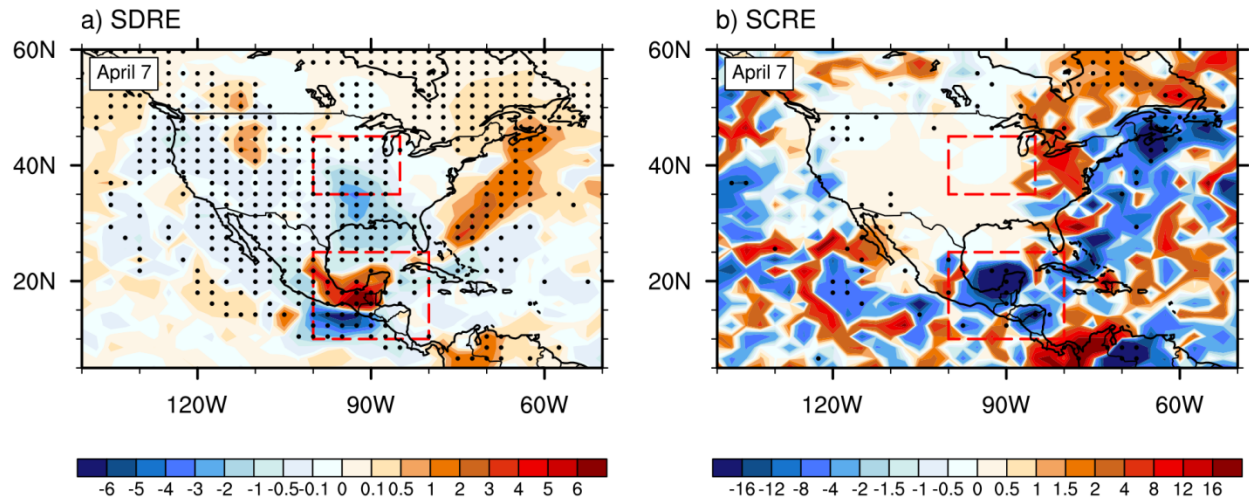


Figure 11. Spatial distributions of ensemble mean fire aerosol a) SDRE and b) SCRE ( $W m^{-2}$ ) on April 7 in the E\_QF simulation. Dots denote grids where fire aerosol effect is statistically significant at the 95% confidence level based on the KS test.

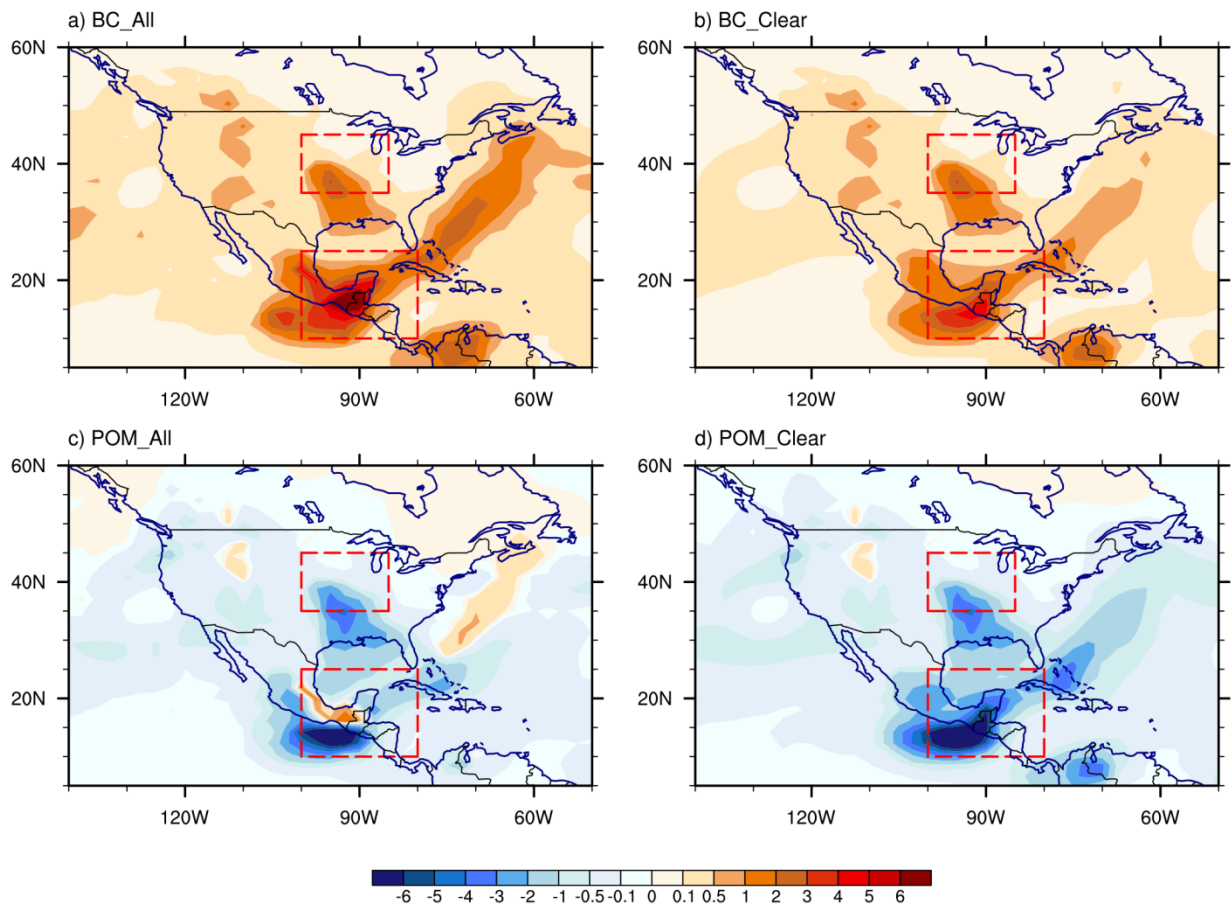


Figure 12. Spatial distributions of fire BC SDRE and fire POM SDRE ( $W m^{-2}$ ) on all-sky and clear-sky conditions on April 7 in the E\_QF simulation.

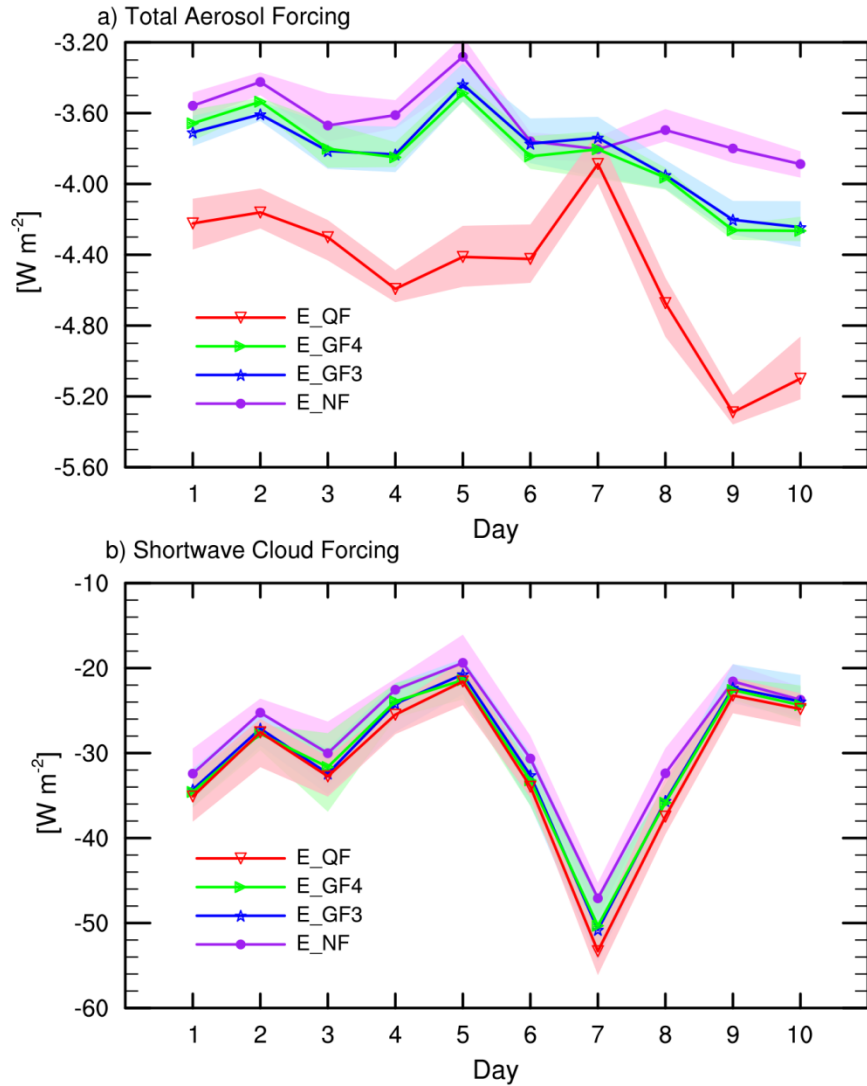


Figure 13. Time series of daily regional mean total a) aerosol forcing and b) cloud forcing in Southern Mexico during Apr.1-10, 2009 in group B simulations. Individual lines indicate ensemble mean values. Shaded areas illustrate the ensemble spread (from minimum to maximum).

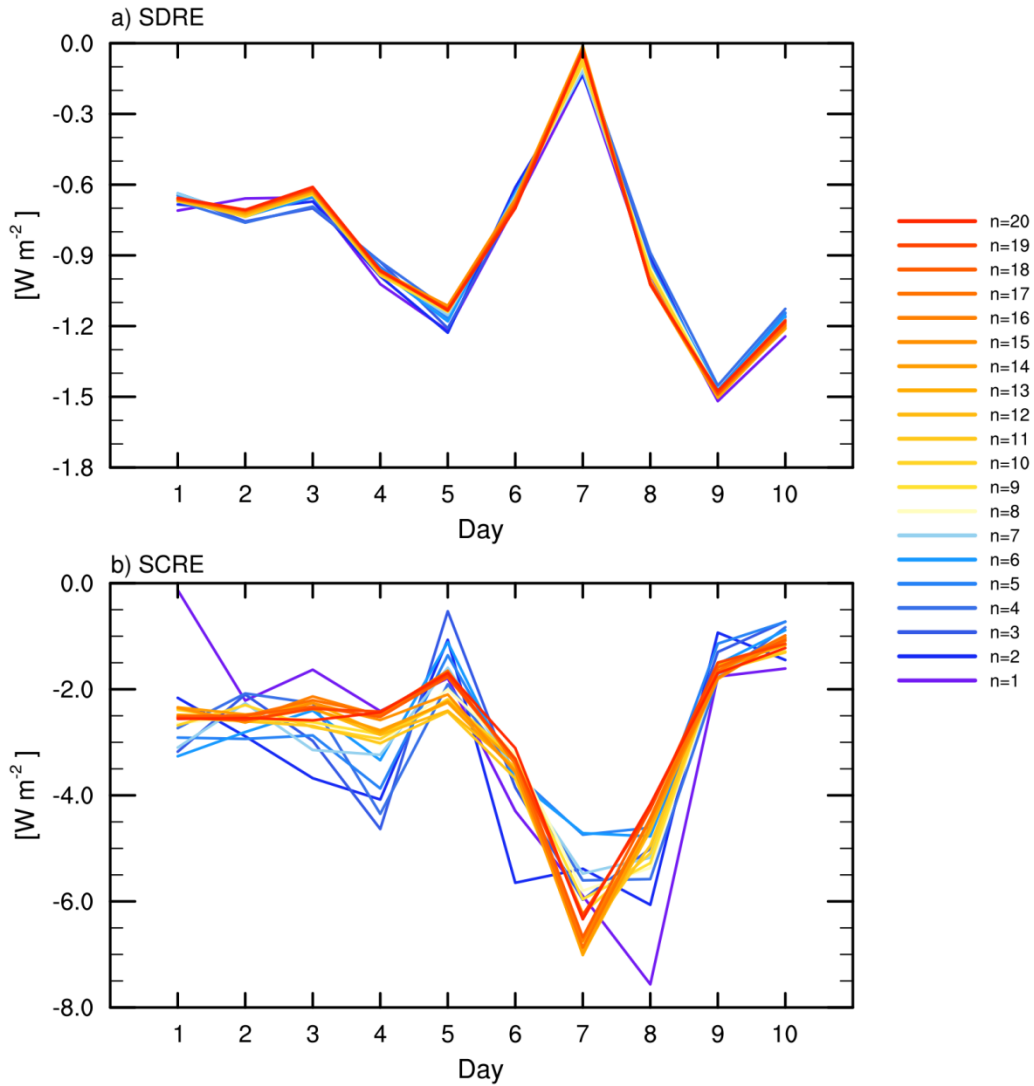
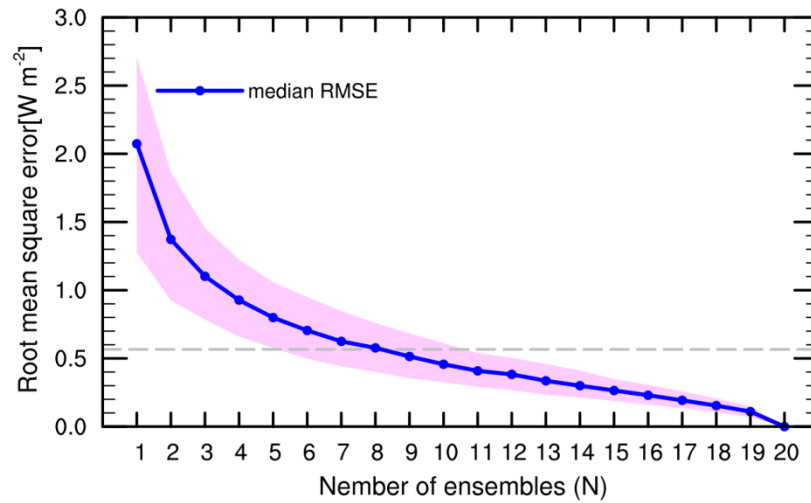


Figure 14. Time series of daily ensemble mean fire aerosol a) SDRE and b) SCRE averaged over Southern Mexico during Apr. 1-10, 2009 in QFED forced ensemble simulations with varying the total number of member numbers (n=1-20).



[Figure 15 Root mean square errors \(RMSE\) of the ensemble mean of the regional mean fire aerosol SCRE during April 1-10 over Southern Mexico in simulations with different total number of ensemble members \(N\). The blue line represents the median RMSE of the 1000 groups \(each group has N members/simulations\). The grey line represents the threshold RMSE. Shaded area denotes the range between the 10<sup>th</sup> and 90<sup>th</sup> percentiles.](#)

Supplemental Materials

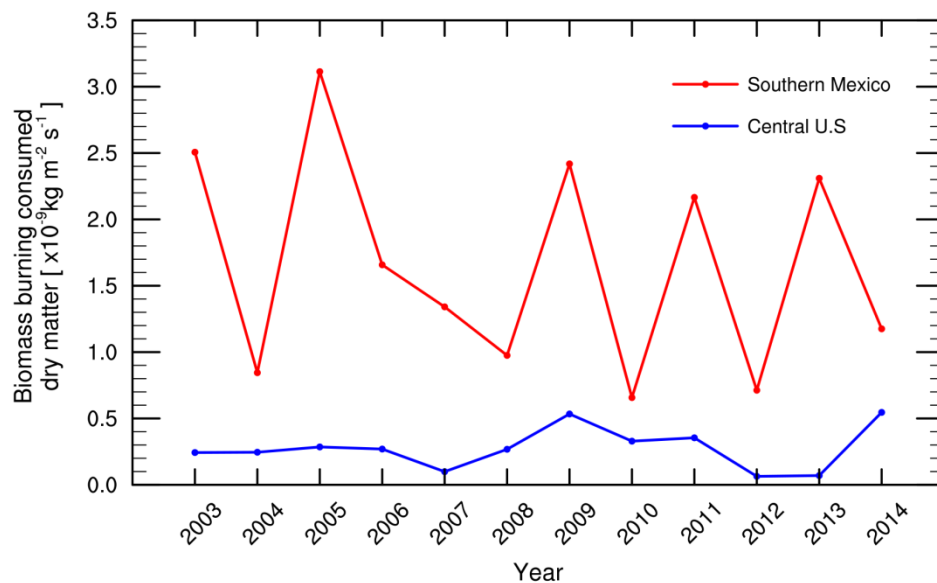


Figure S1. Time series of regional mean biomass burning consumed dry matter during April in central U.S (blue) and Mexico (red) from GFED v4.1.

[Table S1 Regional mean emissions of fire aerosols in April, 2009 from three emission inventories \(Unit:  \$\times 10^{-12}\$  kg m<sup>-2</sup> s<sup>-1</sup>\). Numbers in the parentheses show results averaged in April 1-10.](#)

	<u>BC</u>		<u>OC</u>		<u>SO<sub>2</sub></u>	
	<u>Central</u>	<u>Southern</u>	<u>Central</u>	<u>Southern</u>	<u>Central</u>	<u>Southern</u>
	<u>U.S.</u>	<u>Mexico</u>	<u>U.S.</u>	<u>Mexico</u>	<u>U.S.</u>	<u>Mexico</u>
<u>GFED v3.1</u>	<u>0.25(0.38)</u>	<u>0.69(0.82)</u>	<u>1.82(3.58)</u>	<u>5.60(6.77)</u>	<u>1.35(2.01)</u>	<u>3.69(4.35)</u>
<u>GFED v4.1s</u>	<u>0.23(0.34)</u>	<u>1.17(1.44)</u>	<u>1.75(3.24)</u>	<u>8.80(10.76)</u>	<u>1.21(1.81)</u>	<u>6.25(7.69)</u>
<u>QFED v2.4</u>	<u>2.63(3.29)</u>	<u>3.87(3.87)</u>	<u>23.54(32.25)</u>	<u>36.81(36.58)</u>	<u>14.04(17.59)</u>	<u>20.62(20.65)</u>

Table S2 Regional mean total AOD, fire AOD (difference in total AOD between simulations with and without fire) and the contributions of fire AOD (fire AOD divided by total AOD in the S\_NF simulation) during April, 2009 in group A simulations.

	Central U.S.			Southern Mexico		
	Total AOD	Fire AOD	Percentage	Total AOD	Fire AOD	Percentage
<u>S_NF</u>	<u>0.066</u>			<u>0.130</u>		
<u>S_GF3</u>	<u>0.068</u>	<u>0.002</u>	<u>3.42%</u>	<u>0.141</u>	<u>0.011</u>	<u>8.10%</u>
<u>S_GF4</u>	<u>0.070</u>	<u>0.004</u>	<u>5.63%</u>	<u>0.145</u>	<u>0.015</u>	<u>11.20%</u>
<u>S_QF</u>	<u>0.099</u>	<u>0.033</u>	<u>49.33%</u>	<u>0.194</u>	<u>0.064</u>	<u>48.84%</u>

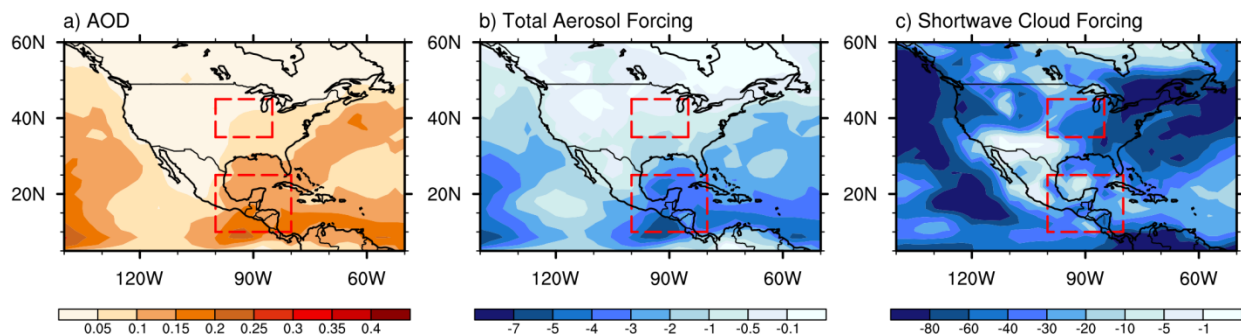


Figure S2. Spatial distributions of 10-day average (Apr. 1-10) ensemble mean a) AOD, b) total aerosol forcing and c) total shortwave cloud forcing(  $W m^{-2}$  ) in the simulation without fire emissions (E\_NF).

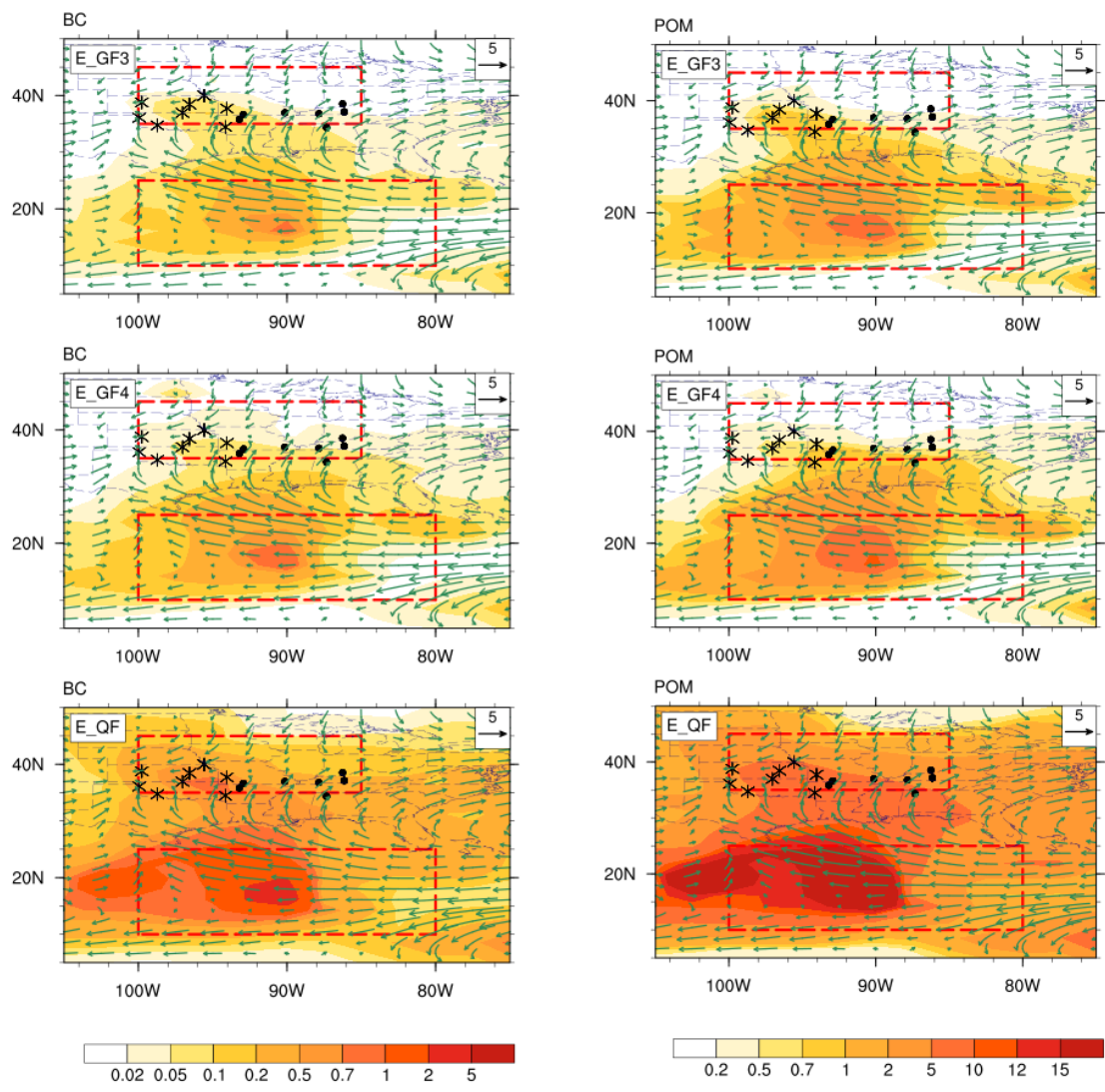


Figure S3. Spatial distributions of April mean fire BC and fire POM burden (shaded) on IMPROVE observation days in group B simulations (E\_GF3/E\_GF4/E\_QF – E\_NF). Vectors denote horizontal winds near 850hPa in group B fire simulations (E\_GF3/E\_GF4/E\_NF). IMPROVE data sites are marked with asterisks for sites near the source region and with dots for sites in the downwind region.



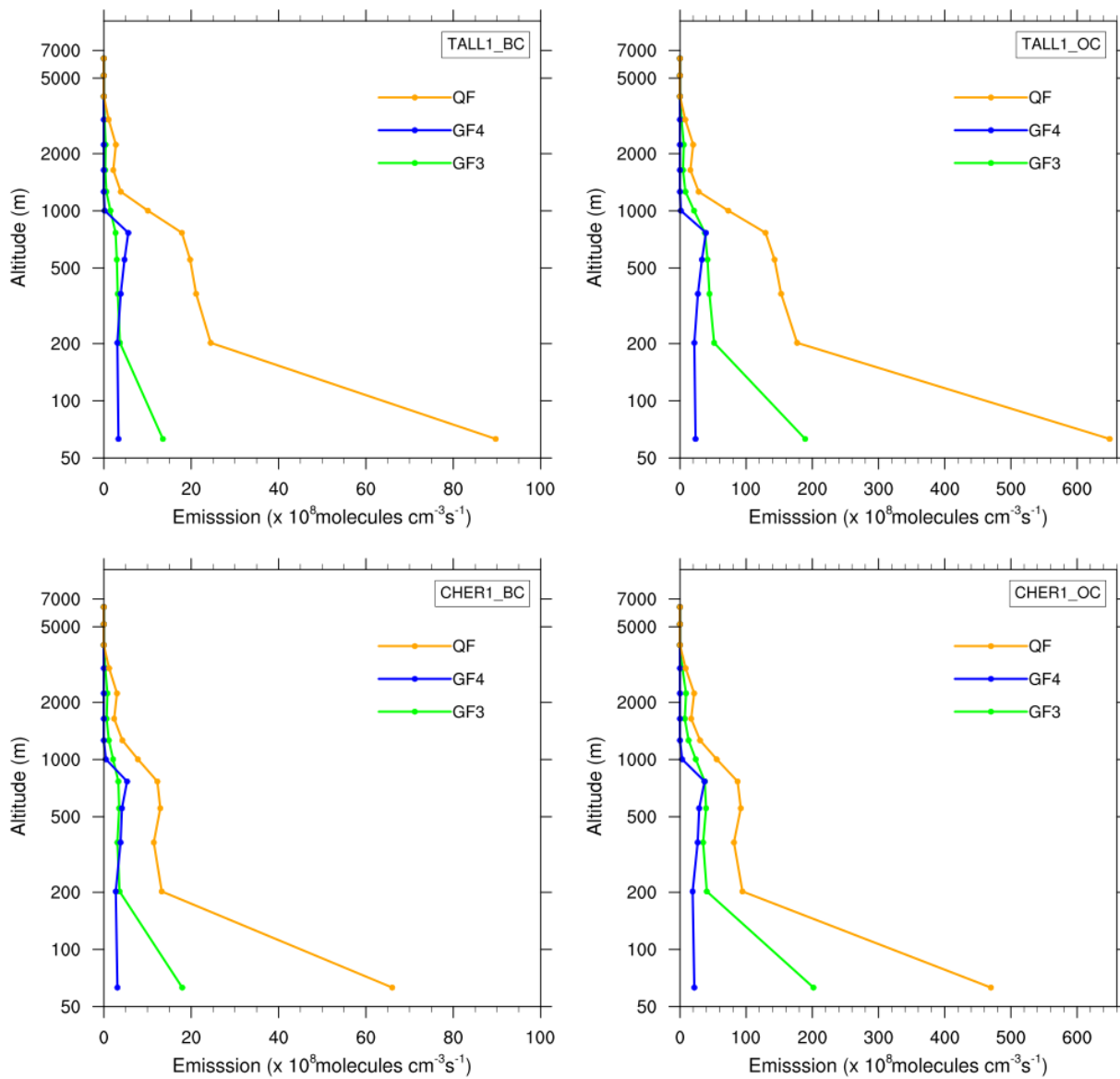


Figure S4. Vertical profiles of fire emissions of BC and OC used in simulations at sites TALL1 ( $38.43^\circ\text{N}$ ,  $96.56^\circ\text{W}$ ) and CHER1 ( $38.77^\circ\text{N}$ ,  $99.76^\circ\text{W}$ ).

Table S3 Regional mean total AOD, fire AOD (differences in AOD between simulations with and without fire) and radiative effects of fire aerosols during April 1-10, 2009 in group B simulations (Unit:  $W m^{-2}$ ). Total fire aerosol radiative effect is decomposed into shortwave direct radiative effect (SDRE), shortwave cloud radiative effect (SCRE), longwave cloud radiative effect (LCRE) and surface albedo effect (SAE).

	<u>Total</u> <u>AOD</u>	<u>Fire AOD</u>	<u>SDRE</u>	<u>SCRE</u>	<u>LCRE</u>	<u>Total SAE</u>
<u>Central U.S.</u>						
<u>E_NF</u>	<u>0.047</u>					
<u>E_GF3</u>	<u>0.050</u>	<u>0.003</u>	<u>0.02</u>	<u>-0.86</u>	<u>0.04</u>	<u>0.02</u>
<u>E_GF4</u>	<u>0.050</u>	<u>0.003</u>	<u>-0.01</u>	<u>-0.39</u>	<u>0.002</u>	<u>-0.003</u>
<u>E_QF</u>	<u>0.08</u>	<u>0.033</u>	<u>-0.10</u>	<u>-0.56</u>	<u>-0.76</u>	<u>0.12</u>
<u>Southern Mexico</u>						
<u>E_NF</u>	<u>0.135</u>					
<u>E_GF3</u>	<u>0.149</u>	<u>0.014</u>	<u>-0.18</u>	<u>-1.91</u>	<u>-0.21</u>	<u>0.06</u>
<u>E_GF4</u>	<u>0.153</u>	<u>0.018</u>	<u>-0.20</u>	<u>-2.06</u>	<u>-0.23</u>	<u>0.11</u>
<u>E_QF</u>	<u>0.202</u>	<u>0.067</u>	<u>-0.86</u>	<u>-3.02</u>	<u>-0.47</u>	<u>0.14</u>

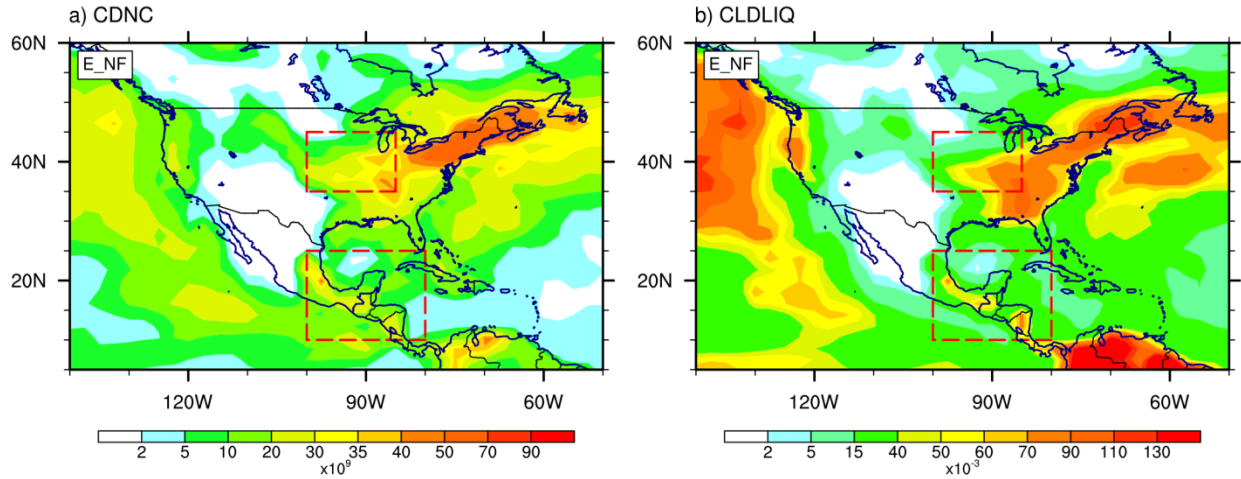


Figure S5. Spatial distributions of 10-day average (Apr. 1-10) ensemble mean a) column-integrated droplet number concentrations ( $\text{m}^{-2}$ ) and b) liquid water path ( $\text{g m}^{-2}$ ) in the E\_NF simulations.

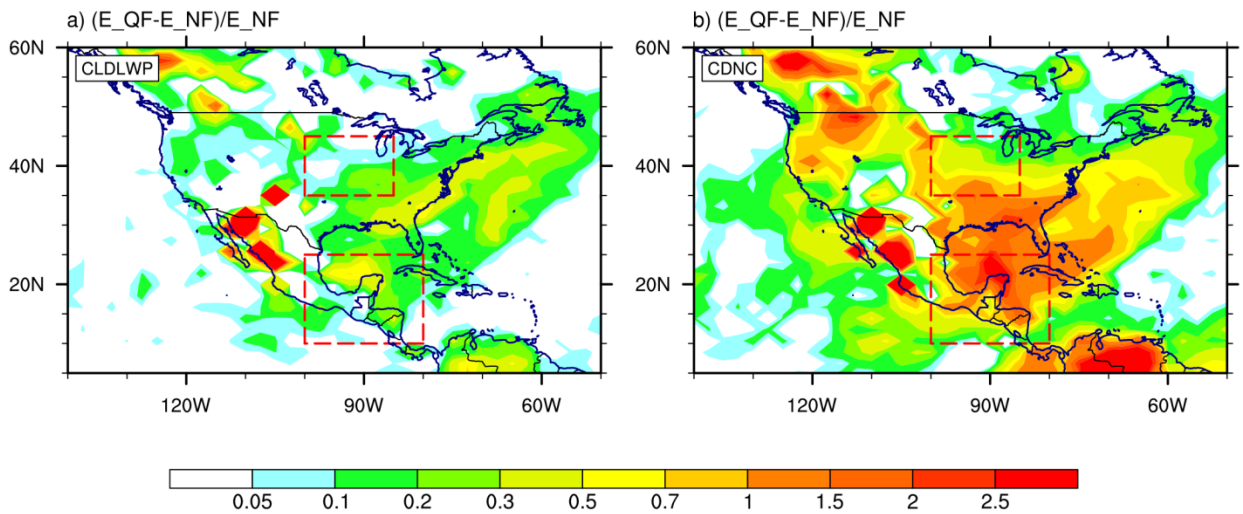


Figure S6. Relative changes of 10-day average ensemble mean cloud properties between the E\_NF and E\_QF simulations. a) cloud liquid water path, b) column-integrated droplet number concentration

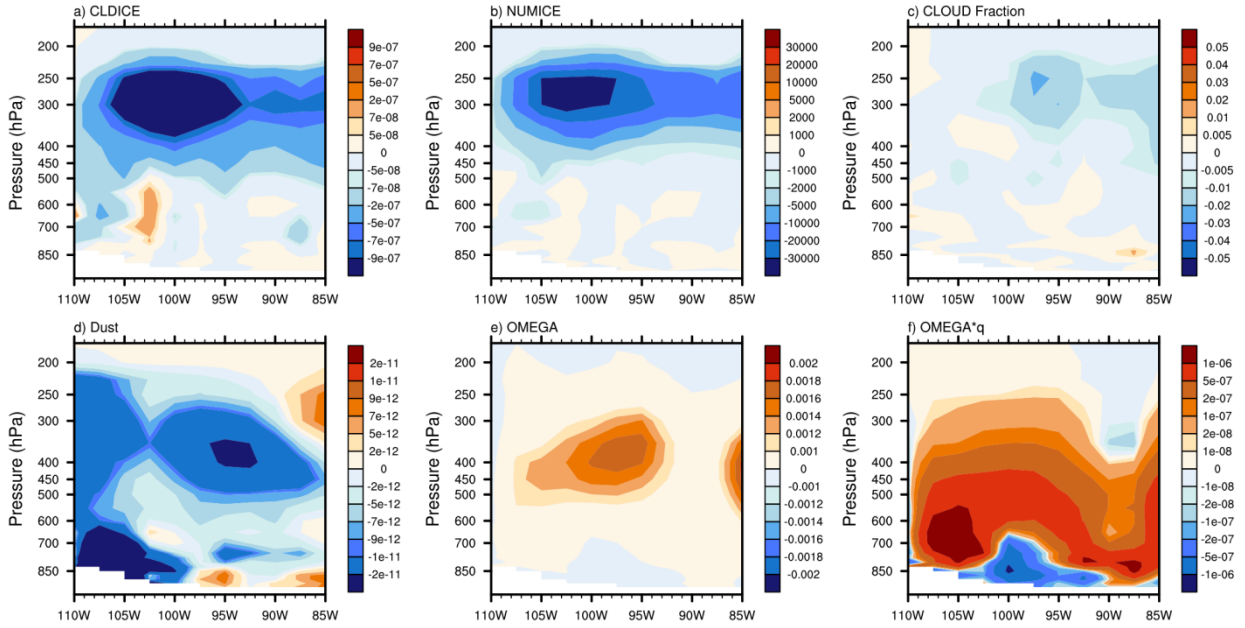


Figure S7. Pressure and longitude distribution of meridional mean ( $40\text{-}45^\circ \text{N}$ ) difference of 10-day average (April 1 -10) ensemble mean between simulation E NF and E QF: a) cloud ice amount ( $\text{kg} \cdot \text{kg}^{-1}$ ) b) cloud ice number concentration ( $\text{kg}^{-1}$ ) c) cloud fraction (1) d) Coarse mode dust concentration ( $\text{kg} \cdot \text{kg}^{-1}$ ) e) vertical velocity ( $\text{Pa} \cdot \text{s}^{-1}$ ) f) vertical moisture transport ( $\text{kg} \cdot \text{kg}^{-1} \cdot \text{Pa} \cdot \text{s}^{-1}$ )

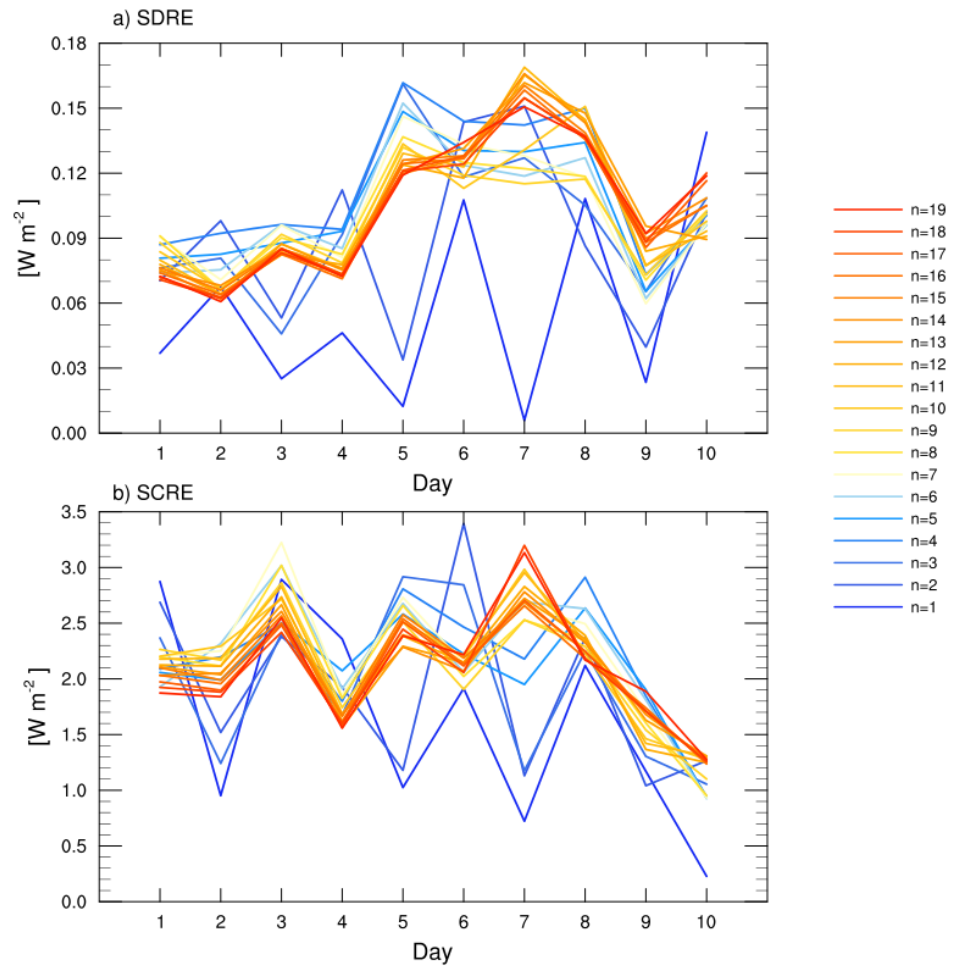


Figure S85. Time series of ensemble spread of daily regional mean fire aerosol a) SDRE and b) SCRE in Southern Mexico during Apr. 1-10, 2009 in QFED forced ensemble simulations with varying the total number of ensemble member (n=1-20).